ICARUS 75, 30–63 (1988)

Convex-Profile Inversion of Asteroid Lightcurves: Theory and Applications

STEVEN J. OSTRO

Jet Propulsion Laboratory, California Institute of Technology, Pasadena, California 91109

ROBERT CONNELLY

Department of Mathematics, Cornell University, Ithaca, New York 14853

AND

MARK DOROGI[1]

Department of Applied and Engineering Physics, Cornell University, Ithaca, New York 14853

Received October 8, 1987; revised December 8, 1987

Convex-profile inversion, introduced by S. J. Ostro and R. Connelly (1984, *Icarus* 57, 443–463), is reformulated, extended, and calibrated as a theory for physical interpretation of an asteroid's lightcurve and then is used to constrain the shapes of selected asteroids. Under ideal conditions, one can obtain the asteroid's "mean cross section" $\underline{C}$, a convex profile equal to the average of the convex envelopes of all the surface contours parallel to the equatorial plane. $\underline{C}$ is a unique, rigorously defined, two-dimensional average of the three-dimensional shape and constitutes optimal extraction of shape information from a nonopposition lightcurve. For a lightcurve obtained at opposition, $\underline{C}$'s odd harmonics are not accessible, but one can estimate the asteroid's symmetrized mean cross section, $\underline{C}_s$. To convey visually the physical meaning of the mean cross sections, we show $\underline{C}$ and $\underline{C}_s$ calculated numerically for a regular convex shape and for an irregular, nonconvex shape. The ideal conditions for estimating $\underline{C}$ from a lightcurve are Condition GEO, that the scattering is uniform and geometric; Condition EVIG, that the viewing-illumination geometry is equatorial; Condition CONVEX, that all of the asteroid's surface contours parallel to the equatorial plane are convex; and Condition PHASE, that the solar phase angle $\phi \neq 0$. Condition CONVEX is irrelevant for estimation of $\underline{C}_s$. Definition of a rotation- and scale-invariant measure of the distance, Ω, between two profiles permits quantitative comparison of the profiles' shapes. Useful descriptors of a profile's shape are its noncircularity, Ω_c, defined as the distance of the profile from a circle, and the ratio β^* of the maximum and minimum values of the profile's breadth function $\beta(\theta)$, where θ is rotational phase. $\underline{C}$ and $\underline{C}_s$ have identical breadth functions. At opposition, under Conditions EVIG and GEO, (i) the lightcurve is equal to $\underline{C}$'s breadth function, and (ii) $\beta^* = 10^{0.4\Delta m}$, where Δm is the lightcurve peak-to-valley amplitude in magnitudes; this is the *only* situation where Δm has a unique physical interpretation. An estimate $\hat{\underline{C}}$ of $\underline{C}$ (or $\hat{\underline{C}}_s$ of $\underline{C}_s$) can be distorted if the applicable ideal conditions are violated. We present results of simulations designed to calibrate the nature, severity, and predictability of such systematic error. Distortion introduced by violation of Condition EVIG depends on ϕ, on the asteroid-centered declinations δ_S and δ_E of the Sun and Earth, and on the asteroid's three-dimensional shape. Violations of Condition EVIG on the order of 10° appear to have little effect for convex, axisymmetric

[1] Current address: Philips ECG, 50 Johnston St., Seneca Falls, NY 13148.

0019-1035/88 $3.00

shapes. Errors arising from violation of Condition GEO have been studied by generating lightcurves for model asteroids having known mean cross sections and obeying Hapke's photometric function, inverting the lightcurves, and comparing $\hat{\underline{C}}$ to $\underline{C}$. The distance of $\hat{\underline{C}}$ from $\underline{C}$ depends on ϕ and rarely is negligible, but values of Ω_c and β^* for $\hat{\underline{C}}$ resemble those of $\underline{C}$ rather closely for a range of solar phase angles ($\phi \sim 20° \pm 10°$) generally accessible for most asteroids. Opportunities for reliable estimation of $\underline{C}_s$ far outnumber those for $\underline{C}$. We have examined how lightcurve noise and rotational-phase sampling rate propagate into statistical error in $\hat{\underline{C}}$ and offer guidelines for acquisition of lightcurves targeted for convex-profile inversion. Estimates of $\underline{C}$ and/or $\underline{C}_s$ are presented for selected asteroids, along with profile shape descriptors and goodness-of-fit statistics for the inverted lightcurves. For 15 Eunomia and 19 Fortuna, we calculate weighted estimates of $\underline{C}$ from lightcurves taken at different solar phase angles.

I. INTRODUCTION

One of an asteroid's most fundamental attributes is its shape, and lightcurves provide the only source of shape information for most asteroids. However, the functional form of a lightcurve is determined by the viewing/illumination geometry and the asteroid's light-scattering properties as well as by its shape, and lightcurves offer less powerful shape constraints than do techniques that resolve asteroids spatially. Ostro and Connelly (1984) introduced a new approach called convex-profile inversion to using a lightcurve to constrain an asteroid's shape, demonstrating that any lightcurve can be inverted to yield a convex profile that, under certain ideal conditions, represents a certain two-dimensional average of the asteroid's three-dimensional shape. The ideal conditions include geometric scattering and equatorial viewing/illumination geometry and will rarely be satisfied exactly for actual lightcurves, so the derived shape constraints will usually contain systematic error.

Therefore, while convex-profile inversion can help to optimize extraction of shape information, proper application of the technique demands an understanding of systematic (as well as statistical) sources of uncertainty. Two objectives of this paper are to explore these effects at some length and then, with a better feel for error sources, to use convex-profile inversion to constrain the shapes of selected asteroids. A third, more general, objective is to present a comprehensive conceptual foundation for the physical interpretation of asteroid lightcurves. This foundation encompasses calibration and application of convex-profile inversion as well as established principles from the oldest lightcurve literature, so let us begin with a review of essential background material in which we emphasize the progression of logic which has led to convex-profile inversion.

II. HISTORICAL BACKGROUND AND REVIEW OF RECENT WORK

A general statement of the lightcurve inversion problem is "Given that a lightcurve is determined by asteroid shape, surface scattering properties, and viewing/illumination geometry, how, if at all, can we isolate these effects and obtain physically interesting information about the asteroid?" In a classic paper, H. N. Russell (1906) offered the first analysis of this problem, investigating in fine detail the information content of lightcurves taken close to opposition, i.e., with the solar phase angle $\phi \sim 0°$. He summarized his results as follows: If an asteroid has been observed at opposition in all parts of its orbit:

(R1) "We can determine by inspection of its light-curves whether or not they can be accounted for by its rotation alone, and, if so, whether the asteroid (a) has an absorbing atmosphere, (b) is not of a convex[2]

[2] An object is convex if the straight line connecting any two points on the boundary is inside the boundary.

form, (c) has a spotted surface, or whether these hypotheses are unnecessary."

(R2) "It is always possible (theoretically) to determine the position of the asteroid's equator, (except that the sign of the inclination remains unknown)." That is, we can find the line of equinoxes, of intersection between the equatorial and orbital planes, and the size of the angle between those planes.

(R3) "It is quite impossible to determine the [three-dimensional] shape of the asteroid. If any continuous convex form is possible, all such forms are possible."

(R4) "In this case we may assume any such form, and then determine a distribution of brightness on its surface which will account for the observed light-curves. This can usually be done in an infinite variety of ways."

(R5) "The consideration of the light-curve of a planet at phases remote from opposition may aid in determining the markings on its surface, but cannot help us find its [three-dimensional] shape."

Despite Russell's skepticism toward prospects for using lightcurves to find an asteroid's three-dimensional shape, he did describe how to test certain hypotheses about shape, scattering law, and albedo distribution. For example, suppose we have found the asteroid's line of equinoxes (R2) and obtained an "equatorial" opposition lightcurve. Russell showed that such a lightcurve's Fourier series cannot have odd harmonics higher than the first if the scattering is geometric,[3] regardless of the albedo distribution; it cannot have *any* odd harmonics if that distribution is uniform. He also showed that if two opposition lightcurves obtained in opposite directions are different, then either the scattering is not geometric or the albedo is not uniform, or both; if the difference is not a sinusoid, then the asteroid's shape is not convex. However, as Russell proved, it is impossible to separate the effects of albedo variation from effects of surface curvature, so *neither the light-scattering properties nor the shape can be modeled uniquely*. Hence, apart from testing the convexity hypothesis, the utility of lightcurves as sources of shape information seemed virtually nil.

More than half a century after Russell's treatise, photoelectric photometry and polarimetry dramatically changed the empirical setting for lightcurve interpretation, demonstrating that with a few notable exceptions the forms of most broadband optical lightcurves seem less sensitive to surface heterogeneity than to gross shape. Moreover, laboratory experiments and theoretical studies disclosed that geometric scattering is likely to be a good approximation for asteroids viewed close to opposition (e.g., French and Veverka 1983) but that the validity of this approximation deteriorates with increasing solar phase angle. Thus, in the absence of evidence to the contrary, the premise that the scattering is uniform and geometric has been the starting point for nearly all efforts to interpret lightcurves physically (e.g., Burns and Tedesco 1979, Harris 1986).

Many researchers further constrain the lightcurve inversion problem by assuming a simple *a priori* shape. The usual choice is a triaxial ellipsoid, whose shape is completely described by the ratios b/a and c/a, with $a \geq b \geq c$ the semiaxis lengths. The equatorial opposition lightcurve of a geometrically scattering ellipsoid (GSE) has brightness extrema in the ratio $a/b = 10^{0.4\Delta m}$, where Δm is the peak-to-valley lightcurve amplitude in magnitudes. A common practice is to take the maximum observed value of Δm as a measure of an asteroid's elongation.

Because GSE lightcurves are easy to calculate, they provide a convenient tool for error-propagation studies (Sections III and IV below) and for pole-direction determinations (e.g., Zappalà and Knežević 1984,

[3] The brightness of a geometrically scattering surface element is proportional to the element's projected, visible, illuminated area.

Scaltriti *et al.* 1978). However, for the purpose of extracting information about an asteroid's shape from its lightcurve, the GSE assumption begs the question. After all, ellipsoids are a subset of axisymmetric shapes, which in turn constitute a small subset of convex shapes and an even smaller subset of plausible asteroid shapes. The GSE assumption forces one to ignore much of the lightcurve's information content, imposing a very particular Fourier structure on any model lightcurve. As shown by Russell and noted above, the equatorial, opposition lightcurve of any object with a geometric scattering law will have no odd harmonics higher than the first. If the asteroid's surface is symmetric about the spin axis then the first harmonic will vanish, leaving only even harmonics in the lightcurve, regardless of viewing aspect. But if, additionally, the asteroid is an ellipsoid, the lightcurve's Fourier structure will be even more restricted: As shown by Connelly and Ostro (1984), the square of the opposition lightcurve of any geometrically scattering ellipsoid has no harmonics except for 0 and 2, regardless of viewing aspect.

How should we interpret the equatorial opposition lightcurve of a uniform, geometrically scattering asteroid which might (by the Fourier test just mentioned) be nonellipsoidal? More generally, *what can any given lightcurve tell us about an asteroid's shape?* Russell wrote that if the scattering is uniform and geometric, then we might "seek to account for the light-changes by the form of the surface alone. But this leads to difficult problems in the theory of surfaces, and will not be attempted here." He pointed out that some of these problems arise because odd harmonics in the expansion of a surface's curvature function will be irretrievable from an opposition lightcurve. He also suggested that the odd harmonics "may sometimes be determined from nonopposition lightcurves." These critical issues were not pursued further for nearly 75 years.

Convex-Profile Inversion: Averages of Asteroid Shapes

Ostro and Connelly (1984) demonstrated that whereas Russell's paper is valid, and indeed it is not possible to find an asteroid's three-dimensional shape from disk-integrated measurements, it is possible to extract shape constraints that are meaningful and that exploit more of the information in the lightcurve. Still, shape constraints from disk-integrated measurements are necessarily much less informative than, say, a stellar-occultation profile, which is a two-dimensional projection of the asteroid's three-dimensional shape. Given an asteroid's lightcurve, the best constraint we can obtain is not a projection of the asteroid's three-dimensional shape, but rather a certain two-dimensional *average* of that shape.

Ostro and Connelly (1984) defined an asteroid's mean cross section $\underline{C}$ as the average of all cross sections $\underline{C}(z)$ cut by planes a distance z above the asteroid's equatorial plane. That definition of the $\underline{C}(z)$ left $\underline{C}$ undefined unless all the $\underline{C}(z)$ are convex. Here, to remedy this situation, we define the $\underline{C}(z)$ as the convex envelopes, or hulls, on the actual surface contours. With this revision, $\underline{C}$ is now clearly defined for any asteroid.

$\underline{C}$ and all the $\underline{C}(z)$ are convex profiles or, in the language of geometry, convex sets. We use underlined, uppercase, italic letters to denote such quantities. As discussed in detail by Ostro and Connelly (1984) and reiterated below, a convex profile can be represented by a radius-of-curvature function or by that function's Fourier series. Deletion of a profile's odd harmonics yields that profile's symmetrization. For example, an asteroid's symmetrized mean cross section $\underline{C}_s$ has the same even harmonics as $\underline{C}$ but no odd harmonics.

Figure 1 shows $\underline{C}$ and $\underline{C}_s$ for two three-dimensional, styrofoam models, calculated by applying formulas in Appendix A of Ostro and Connelly (1984) to measurements of photographs of those objects. Several pho-

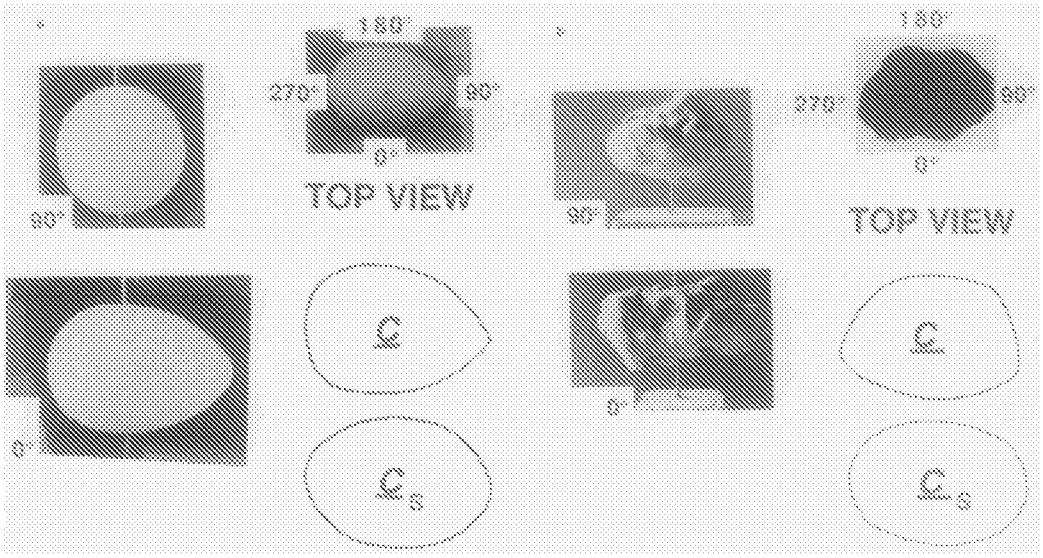

FIG. 1. Values of the mean cross section for (a) an egg-shaped object and (b) an irregular, nonconvex object.

tographs of each model are shown to convey visually the relation between three-dimensional shape and the two-dimensional averages accessible from lightcurves.

There are four ideal conditions for estimating $\underline{C}$ from a lightcurve:

Condition GEO: The scattering is uniform and geometric.

Condition EVIG: The viewing-illumination geometry is equatorial, that is, the asteroid-centered declinations δ_S and δ_E of the Sun and Earth are zero.

Condition CONVEX: All of the asteroid's surface contours parallel to the equatorial plane are convex.

Condition PHASE: The solar phase angle ϕ is known and does not equal 0° or 180°.

The last condition states that we cannot find $\underline{C}$ from an opposition lightcurve and arises for the following reason. Each coefficient in the Fourier series for $\underline{C}$'s radius-of-curvature function is found from the corresponding coefficient in the Fourier series for the lightcurve. However, we cannot use an opposition lightcurve to find $\underline{C}$'s odd harmonics because, as Russell showed, an opposition lightcurve has no odd harmonics if Conditions GEO and EVIG are satisfied. (If $\underline{C}$ contains odd harmonics, then lightcurve odd harmonics can be introduced away from opposition via the rotational-phase dependence of the fraction of the visible projected area that is illuminated. At opposition, no shadows are visible, so that fraction is unity regardless of rotational phase, and the odd harmonics vanish.)

Although we cannot estimate $\underline{C}$ from an opposition lightcurve, we can estimate $\underline{C}$'s even harmonics and hence its symmetrization, $\underline{C}_S$. Estimation of $\underline{C}_S$ from opposition lightcurves is less "burdened" by ideal conditions than is estimation of $\underline{C}$ from nonopposition lightcurves, for three reasons. First, for estimation of $\underline{C}$, Condition CONVEX ensures the absence of visible shadows between the limb and the terminator, which might distort determination of $\underline{C}$. However, at opposition, there are no visible shadows, so Condition CONVEX is irrelevant and C_S can be estimated reliably as long as Conditions GEO and EVIG are satisfied.

Second, Conditions GEO and EVIG are "satisfied more easily" for opposition lightcurves than for nonopposition lightcurves. As noted above, the geometric scattering

approximation is more valid at opposition than at large solar phase angles. Condition EVIG can be satisfied at large phase angles only if the pole lies nearly normal to the Earth–asteroid–Sun *plane*, but is satisfied at any opposition occurring when the asteroid is at an equinox, i.e., with the pole normal to the Earth–asteroid *line*. Hence, geometry dictates that opportunities to estimate $\underline{C}_s$ far outnumber opportunities to estimate $\underline{C}$.

Third, to assess how close the viewing/illumination geometry is to equatorial for a given nonopposition lightcurve, one must know the asteroid's *pole direction;* for an opposition lightcurve it is sufficient to know just the location of the asteroid's *line of equinoxes*.

Ostro and Connelly (1984) showed that calculation of a mean-cross-section estimate $\hat{\underline{C}}$ from a lightcurve can be approached by weighted-least-squares optimization subject to inequality constraints. In this paper, we use the term "convex-profile inversion" to denote our theory for the information content of lightcurves as well as the computational technique for estimating mean cross sections.

None of the first three ideal conditions are likely to be satisfied exactly for an actual lightcurve. However, the important issue is the extent to which their violation degrades the accuracy of a mean-cross-section estimate. As noted above, key objectives of this paper are to calibrate convex-profile inversion's sensitivity to systematic and statistical sources of error and then to use convex-profile inversion to constrain the shapes of selected asteroids. In the next section we briefly review the mathematics of convex-profile inversion and introduce techniques for describing, comparing, and manipulating profiles. In Section IV we explore the manner in which departure from ideal conditions makes $\hat{\underline{C}}$ deviate from $\underline{C}$. We have tried to maintain at least a modicum of realism in evaluating sources of systematic error. For example, special attention is paid to the distortion caused by nongeometric scattering, and in calibrating this distortion we have relied heavily on Hapke's (1981, 1984, 1986) theory for a realistic description of the optical properties of asteroid surfaces. On the other hand, our calibrations have not been exhaustive; we have not examined coupled effects due to simultaneous violation of two or more ideal conditions, and we have simplified as much as possible our modeling of three-dimensional shapes. Nonetheless, our work does provide a guide to both the power and the limitations of convex-profile inversion. We argue that systematic errors in estimation of $\underline{C}$ and $\underline{C}_s$ are not insurmountable and that their severity often can be assessed *a priori* and/or *a posteriori*.

In Section V we briefly examine how noise, sampling rate, and rotational phase coverage propagate into statistical error in mean-cross-section estimation. Then, having calibrated various sources of uncertainty in convex-profile inversion, we apply it in Section VI to an assortment of asteroid lightcurves. Finally we summarize all our results and offer strategies for future efforts in the acquisition and physical interpretation of asteroid lightcurves.

III. CONVEX-PROFILE INVERSION MATHEMATICS

The power of convex-profile inversion rests on the fact that when the ideal conditions hold, the three-dimensional lightcurve inversion problem, which cannot be solved uniquely, collapses into a two-dimensional problem that can. The geometry of the two-dimensional problem is shown in Fig. 2, drawn for $\phi = 30°$. The asteroid is a convex profile whose brightness $I(\theta)$ at rotational phase θ is proportional to the orthogonal projection toward Earth of the visible, illuminated portion of the profile.

At *opposition,* the visible portion of the profile is fully illuminated; the projection of this curve is called the profile's width, or "breadth," in the direction of Earth, and the lightcurve is proportional to the breadth function $\beta(\theta)$. Unless this function is con-

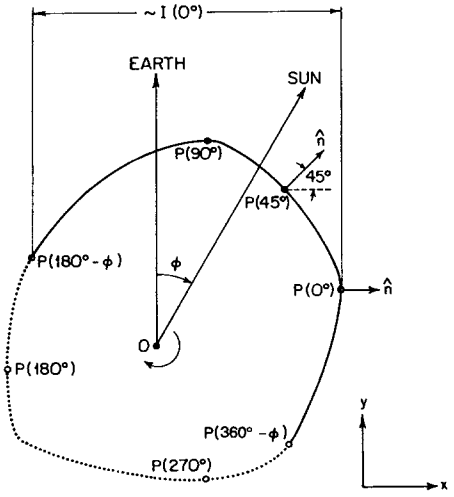

FIG. 2. Geometry for two-dimensional asteroid lightcurve inversion. The asteroid is a convex profile rotating clockwise and is shown at rotational phase $\theta = 0°$. The solar phase angle ϕ is indicated, as are the asteroid's illuminated (solid) and unilluminated (dotted) portions. The asteroid's scattering law is geometric; i.e., the observed brightness is proportional to the orthogonal projection toward Earth of the visible, illuminated length $I(\theta)$. The point $P(\theta)$ is on the receding (left-hand) limb and the outward normal $\hat{\mathbf{n}}$ at $P(\theta)$ points in the positive x direction when the rotational phase is θ. Reproduction of Fig. 1 of Ostro and Connelly (1984).

stant, it is periodic with a period equal to 180° or an integral fraction thereof—the lightcurve has no odd harmonics. (This is why most asteroid lightcurves, which are rarely obtained very far from opposition, are dominated by even harmonics.) The second harmonic dominates the higher even harmonics unless the profile possesses symmetry akin to that of regular convex polygons, in which case the lightcurve's fundamental can be a higher even harmonic. (Asteroids are unlikely to have such symmetry, and this is why most asteroid lightcurves are dominated by the second harmonic.)

The lightcurve's Fourier series can be expressed either as

$$I(\theta) = \sum_{n=0}^{\infty} (a_n \cos n\theta + b_n \sin n\theta)$$

or as

$$I(\theta) = \sum_{n=-\infty}^{\infty} \underline{c}_n e^{in\theta},$$

where

$$\underline{c}_{\pm n} = (a_n \mp ib_n)/2.$$

Define $P(\theta) = [x(\theta), y(\theta)]$ as the point on the curve that would be on the receding limb if the asteroid were at rotational phase θ. In this normal-angle parameterization, the outward normal to the curve at $P(\theta)$ points in the positive x direction at rotational phase θ. Let $r(\theta) = ds/d\theta$ be the radius of curvature of the profile at $P(\theta)$, where $1/r(\theta)$ is the curvature at $P(\theta)$ and $s = s(\theta)$ is arc length defined by

$$(ds/d\theta)^2 = (dx/d\theta)^2 + (dy/d\theta)^2.$$

Then

$$x(\theta) = x(0) - \int_0^{\theta} r(t) \sin t \, dt$$

and

$$y(\theta) = y(0) + \int_0^{\theta} r(t) \cos t \, dt.$$

Ostro and Connelly (1984) define the Fourier series for the radius of curvature function as

$$r(\theta) = \sum_{n=-\infty}^{\infty} \underline{d}_n e^{in\theta}$$

and show that the profile can be found from the lightcurve because

$$\underline{d}_n = \underline{c}_n/\underline{v}_n, \qquad (1)$$

where $\underline{v}_n$ is a known function (Fig. 3) of ϕ. The profile will be closed only if $\underline{d}_{\pm 1} = 0$ and it will be convex only if a set of N linear constraints, $r(2\pi k/N) > 0$ for $1 \leq k \leq N$, are satisfied. In practice, convex-profile inversion finds that profile $\hat{\underline{C}}$ which provides the least-squares estimator for $\underline{C}$ by finding that vector $\hat{\mathbf{x}}$ of Fourier coefficients that satisfies the constraints and is as close as possible to the (unconstrained) vector $\hat{\mathbf{x}}$ of

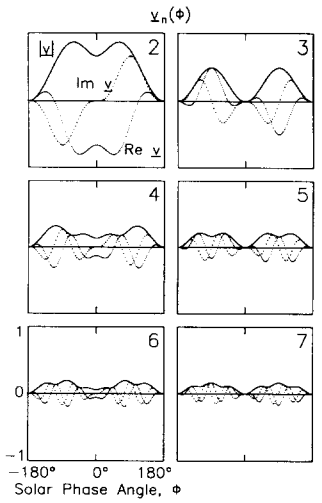

FIG. 3. The function $\underline{v}_n(\phi)$, discussed in the text, is plotted vs solar phase angle ϕ for values of the harmonic index n from 2 through 7. The following expressions for $\underline{v}_n$ are valid for $n \neq \pm 1$; see Section II.A of Ostro and Connelly (1984). If $0 \leq \phi < \pi$, then $2\underline{v}_n = e^{i(n-1)(\pi-\phi)}/(n-1) - e^{i(n+1)(\pi-\phi)}/(n+1) - 2/(n^2-1)$. If $-\pi < \phi \leq 0$, then $2(n^2-1)\underline{v}_n = (n-1)e^{-i(n+1)\phi} - (n+1)e^{-i(n-1)\phi} + 2(-1)^{n+1}$.

Fourier coefficients fit to the data. The lightcurves derived from $\hat{\mathbf{x}}$ and $\hat{\mathbf{x}}$ are, in vector notation, $\hat{\mathbf{y}}$ and $\hat{\mathbf{y}}$.

Truncation of Fourier Series

As discussed by Ostro and Connelly (1984), truncation of Fourier series limits the fidelity with which convex-profile inversion can reproduce profiles with flat sides or sharp corners. We employ Fourier series containing 10 harmonics throughout this paper; series this long adequately represent all lightcurves discussed herein. We note that lightcurves with significant energy in harmonics higher than 10 are rare, and we speculate that the mean cross sections of actual asteroids generally lack extremely flat sides and very sharp corners.

Sign of the Solar Phase Angle

As shown in Fig. 2, the solar phase angle is measured *from* the Earth direction **E** *to* the Sun direction **S** in the same rotational sense as the asteroid's rotation. We adhere to the semantic convention that ϕ satisfies $0° \leq |\phi| \leq 180°$, so $\phi \neq 0$ is positive if the asteroid rotates through $|\phi|$ from **E** to **S** or negative if it rotates through $|\phi|$ from **S** to **E**. For example, in Fig. 2, if the directions of the Earth and Sun were interchanged, ϕ would equal $-30°$. Clearly, for any given Sun–Earth–asteroid geometry, the sign of ϕ is determined by the sense of rotation. Thus convex-profile inversion of a nonopposition lightcurve is sensitive to the sense of rotation, and using the wrong sign of ϕ can distort $\hat{C}$; see Fig. 3 of Ostro and Connelly (1984). However, we suspect that if prior knowledge of an asteroid's pole direction is adequate to guarantee that the asteroid-centered declinations of the Sun and Earth are both close to zero for a given nonopposition lightcurve, then in many cases the data (lightcurve, radar, or whatever) used to constrain the pole direction will be adequate to permit reliable determination of rotation sense, too.

Quantitative Description of Profiles

We often will wish to quantify relationships between profiles to supplement verbal descriptions and subjective comparisons. Following Richard and Hemami (1974) and Sato and Honda (1983), we define the distance Ω between any two profiles $\underline{P}_1$ and $\underline{P}_2$ as

$$\Omega = 10 \min_{\theta} |\underline{d}_1/d_{10} - \Theta\underline{d}_2/d_{20}|,$$

where $\underline{d}_j$ is the vector of complex Fourier coefficients in the expansion of $\underline{P}_j$'s radius-of-curvature function; d_{j0} is the constant, or zero-harmonic term, in that expansion; and the diagonal matrix Θ rotates d_{2n} by $e^{in\theta}$. This distance measure is rotation invariant and scale invariant.

The meaning of Ω can be visualized as follows. If our Fourier series are truncated to M harmonics, $\underline{d}_j$ will have $2M + 1$ elements, so $\underline{d}_1$ and $\underline{d}_2$ define two points in a $(2M + 1)$-dimensional space, and it is easy to calculate the distance between them.

However, $\underline{d}_j$ determines $\underline{P}_j$'s circumference (i.e., its size) and rotational orientation as well as its shape. Therefore, we define Ω as the distance between $\underline{d}_1$ and $\underline{d}_2$ when $\underline{P}_1$ and $\underline{P}_2$ are scaled to the same size and rotated as much into alignment with each other as possible.

In describing interprofile distances, we will use the following scale:

Distance (Ω)	Verbal description
≤ 2	Nearly identical
3–4	Similar but not the same
5–6	Different
7–8	Very different
≥ 9	Radically different

We also define a profile's "noncircularity" Ω_C as its distance from a circle, and a profile's breadth ratio $\beta^* \geq 1$ as the ratio of the profile's maximum breadth to its minimum breadth. Figure 4 plots Ω_C vs β^* for ellipses and shows the locations of various profiles in this two-parameter space, as well as some interprofile distances. Table I lists symbols used frequently in this paper.

TABLE I

GLOSSARY OF SYMBOLS

$\underline{C}$	Mean cross section
$\underline{C}_S$	Symmetrized mean cross section
$\hat{\underline{C}}$	Estimate of $\underline{C}$
$\hat{\underline{C}}_S$	Estimate of $\underline{C}_S$
ϕ	Solar phase angle
Δm	Lightcurve peak-to-valley amplitude
δ_E	Asteroid-centered declination of Earth
δ_S	Asteroid-centered declination of the Sun
β^*	Breadth ratio; ratio of a profile's maximum and minimum widths
Ω	Distance between two profiles
Ω_C	Noncircularity; distance of a profile from a circle
Ω_E	Error distance, between $\hat{\underline{C}}$ and $\underline{C}$ (or between $\hat{\underline{C}}_S$ and $\underline{C}_S$)
Ω_S	Symmetrization distance, between $\hat{\underline{C}}$ and $\hat{\underline{C}}_S$ (or between $\underline{C}$ and $\underline{C}_S$)

IV. SENSITIVITY TO DEPARTURE FROM IDEAL CONDITIONS

A. *Violation of Condition EVIG*

As a first step in studying how departures from ideal conditions can introduce system-

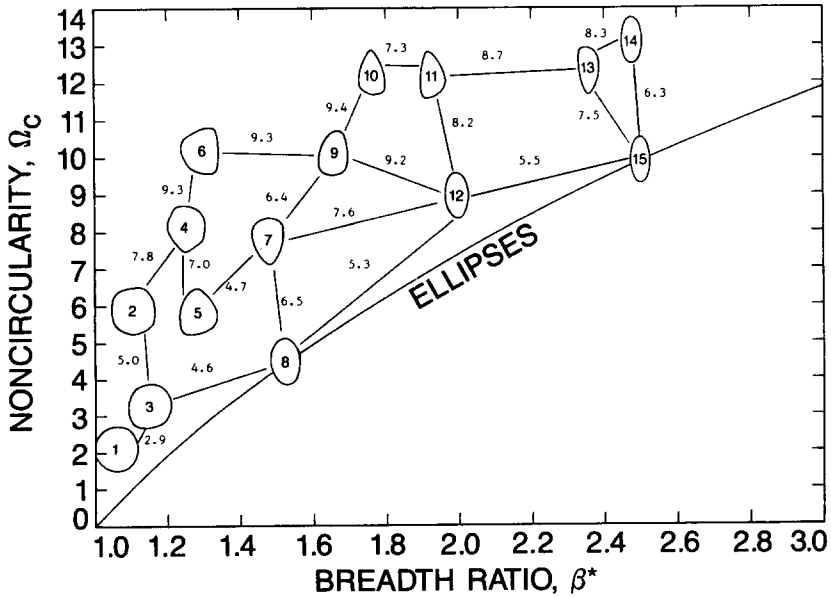

FIG. 4. Shape descriptors for convex profiles. Each profile's noncircularity Ω_C and breadth ratio β^* is indicated by the profile's position. Note the locus of ellipses. The interprofile distance Ω, defined in the text, is indicated for selected pairs of profiles.

atic error in $\hat{\underline{C}}$ or $\hat{\underline{C}}_S$, we examine effects of nonequatorial viewing/illumination geometry. For any given asteroid, the proximity of $\hat{\underline{C}}$ to $\underline{C}$ for a lightcurve obtained when $\delta_E \neq 0$ or $\delta_S \neq 0$ will be a function of δ_E, δ_S, and ϕ. We have studied this particular source of systematic error by inverting lightcurves generated analytically for geometrically scattering ellipsoids within the parameter space:

$$10° \leq \phi \leq 80°$$

$$0.2 \leq b/a \leq 0.4$$

$$0.05 \leq c/a \leq b/a.$$

For given values of b/a, c/a, and ϕ, the field of possible values of δ_E and δ_S is conveniently displayed in a plot of δ_S vs $(\delta_E - \delta_S)$. Figure 5 shows several contours of constant δ_E and of constant δ_S in this plane. Note that the Earth is north of the equator outside the stippled zone. The figure shows results of our simulations for illustrative two-dimensional cuts through the five-dimensional parameter space.

Under Condition EVIG (at the origin of the figures, where $\delta_E = \delta_S = 0$), $\hat{\underline{C}}$ is nearly indistinguishable from the asteroid's mean cross section $\underline{C}$, which is an ellipse with axis ratio a/b. However, under extremely nonideal viewing/illumination geometry, $\hat{\underline{C}}$ is not necessarily elliptical and has breadth extrema not necessarily in the ratio b/a. The distortion in each $\hat{\underline{C}}$ in Fig. 5 is quantified by the "error distance" Ω_E between $\hat{\underline{C}}$ and $\underline{C}$. It worsens with increasing ϕ, a/b, or a/c and is most severe when $|\delta_E|$, $|\delta_S| > 10°$ and δ_S is between 0° and δ_E. The distortion is minimal when *either* $|\delta_E|$, $|\delta_S < 10°$ *or* δ_E is between 0° and $-\delta_S$, i.e., in the triangular region labeled MIN in Fig. 5. Outside those regions, violation of Condition EVIG often makes $\hat{\underline{C}}$ more circular than $\underline{C}$. This result, which is consistent with the well-known reduction in lightcurve amplitude with decreasing aspect angle for opposition lightcurves of geometrically scattering ellipsoids and a variety of other shapes (Barucci and Fulchignoni 1982, 1984), arises from the constant illumination and visibility of a polar region.

From the viewpoint of convex-profile inversion, nonequatorial viewing/illumination geometry prevents the "clean" collapse of the lightcurve inversion problem from three dimensions to two dimensions. It seems unlikely that many asteroids are as long and flat as our most extreme examples, and in this respect our figures might exaggerate the distortion caused by nonequatorial viewing/illumination geometry. On the other hand, distortion for nonaxisymmetric and highly irregular shapes might be much more severe than for ellipsoids. Note that in the minimum-distortion region in the figure, the constantly illuminated pole is not visible and vice versa, so neither polar region contributes to the lightcurve. $\hat{\underline{C}}$ resembles $\underline{C}$ in this region because $\underline{C}(z)$ has a constant shape for an ellipsoid, a situation unlikely to hold for most asteroids. Hence, even if EVIG were the only violated condition, it would probably be wise to interpret the simulations described here as establishing a lower bound on the systematic error in $\hat{\underline{C}}$.

B. Violation of Condition GEO

How much is $\hat{\underline{C}}$ distorted if the scattering is nongeometric? Our strategy in answering this question is to (i) assume that the other ideal conditions are satisfied; (ii) generate lightcurves for an asteroid with a known shape and a realistic scattering law; (iii) use convex-profile inversion to obtain an estimate, $\hat{\underline{C}}$, of the asteroid's mean cross section $\underline{C}$; and (iv) compare $\hat{\underline{C}}$ to $\underline{C}$. For the time being, let us also assume that the asteroid's three-dimensional shape is a convex cylinder, that is, that $\underline{C}(z)$ is constant and congruent with $\underline{C}$. These assumptions reduce the problem's dimensionality to two, letting us treat the asteroid's surface as a convex profile. For convenience we model an asteroid as a convex polygon with 360 sides. The orientation and length of each side is known, so it is easy to calculate the asteroid's lightcurve for an arbitrary

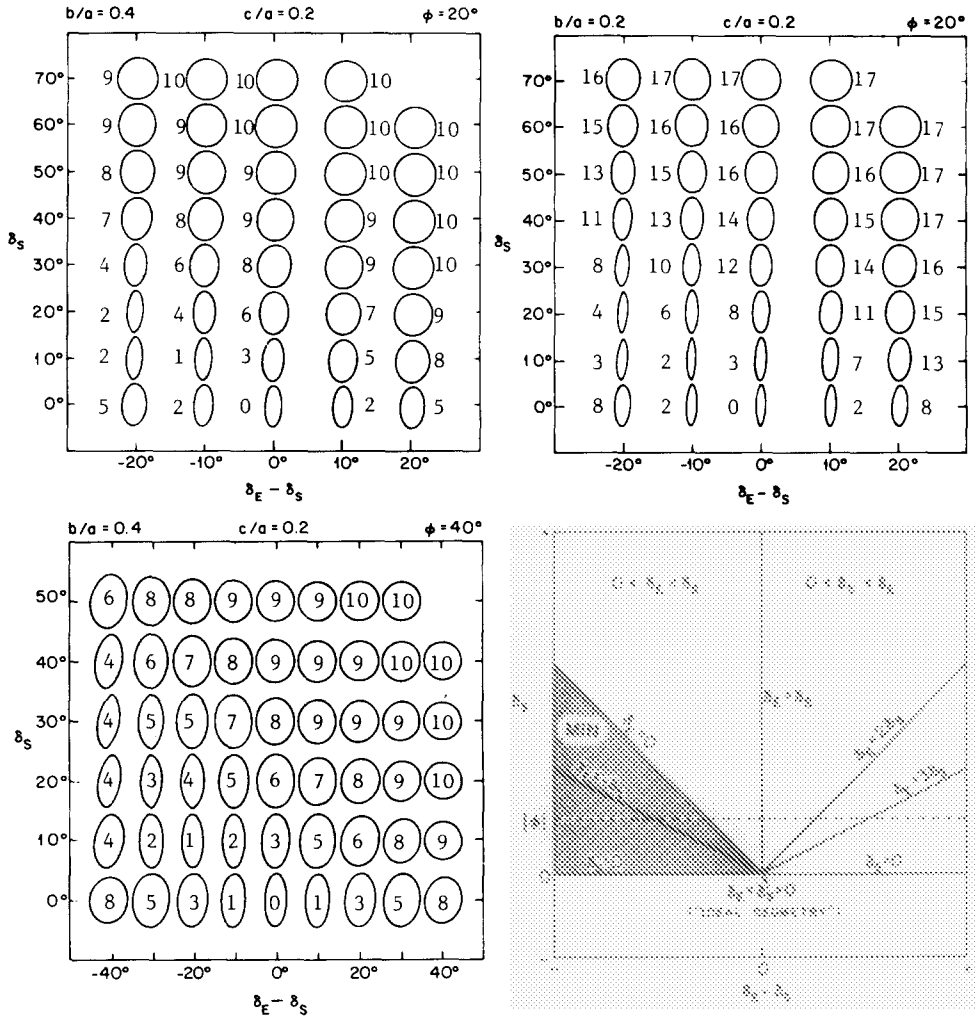

FIG. 5. Systematic errors due to nonequatorial viewing/illumination geometry (violation of Condition EVIG). Convex profile inversion has been applied to lightcurves generated for geometrically scattering ellipsoids, for various values of the asteroid-centered declinations δ_S and δ_E of the Sun and Earth. The field of viewing/illumination geometries is displayed in plots with δ_S on the ordinate and $(\delta_E - \delta_S)$ on the abscissa. The bottom right-hand drawing identifies several regions and lines in that coordinate system. Note that the Earth is north of the equator everywhere except within the shaded area. The three arrays of profiles show estimates $\hat{\underline{C}}$ of the mean cross section $\underline{C}$ (shown as the ellipse at the origin) for three different sets of choices for the solar phase angle ϕ and the ellipsoid's axis ratios b/a and c/a. The "error distance" Ω_E, of $\hat{\underline{C}}$ from $\underline{C}$, is given for each profile. Distortion due to violation of Condition EVIG is minimal within the region labeled "MIN."

photometric function. (By virtue of Condition EVIG, the flat polar surfaces do not contribute to the lightcurve.)

Hapke's (1981, 1984, 1986) theory of diffuse scattering from a particulate medium lets one express the contribution $\underline{dI}$ to an asteroid's brightness from light reflected from a surface areal element $\underline{dA}$ as

$$dI = r_R[\theta_i, \theta_e, |\phi|; w, h, S(0), \bar{\theta}, b_{leg}, c_{leg}]\, dA \cos\theta_e$$

where the reflectance r_R is defined in the

cited references, θ_i and θ_e are the angles of incidence and emergence, and six parameters describe the surface properties. The parameter w is the average single-scattering albedo. The opposition effect is described by the parameters h and $S(0)$; h depends on the regolith's porosity and particle size distribution, and $S(0)$ is the fraction of light scattered from close to a particle's surface at $\phi = 0$. Effects of macroscopic surface roughness are parameterized by the average slope $\bar{\theta}$, measured with respect to the mean surface, of surface facets unresolved by the detector. Following Helfenstein and Veverka (1987), we write the average, single-particle, angular scattering function as

$$P(\phi) = 1 + b_{leg} \cos \phi + c_{leg}(1.5 \cos^2 \phi - 0.5).$$

Those authors estimated values of the six Hapke parameters for dark, average, and bright terrains on the Moon. In our calculations, we adopt their results for average terrain: $w = 0.25$, $h = 0.06$, $S(0) = 0.78$, $\bar{\theta} = 20.6°$, $b_{leg} = 0.33$, and $c_{leg} = 0.37$. Our results are essentially insensitive to variation in these values over ranges much larger than those spanned by their results for the three lunar terrain classes.

For a geometric scattering law (r_R = constant), convex-profile inversion yields $\underline{C}_s$ at opposition and $\underline{C}$ away from opposition. Figure 6 shows $\underline{C}$ and $\underline{C}_s$ for each of 15 model asteroids, as well as $\hat{\underline{C}}$ or $\hat{\underline{C}}_s$ estimated from lightcurves generated under the assumption of Hapke scattering at $\phi = 0°$, 2°, 5°, 10°, 20°, 30°, 50°, and 90°. The figure also lists for each profile the breadth ratio β^*, the error distance Ω_E from $\underline{C}$ (or $\underline{C}_s$), and the noncircularity Ω_c. (The 15 model asteroids' mean cross sections are plotted in Fig. 4.)

Figure 7a plots Ω_E for each object. Figure 7b plots the average value of Ω_E for all 15 objects, the average value for the only three objects (No. 8, 14, and 15) with negligible energy in odd harmonics, and the average value for the 12 remaining objects. These figures demonstrate that the difference between $\hat{\underline{C}}$ and $\underline{C}$ generally depends on the solar phase angle. At opposition, the scattering is sufficiently close to geometric that $\underline{C}_s$ is very accurately determined. (In fact, for ϕ less than about 10°, one can estimate the symmetrized mean cross section quite reliably, with Ω_E rarely as large as 5.) However, for very small phase angles (2° and 5° in the figures), Ω_E is extremely large for all profiles except objects No. 8, 14, and 15; object No. 12 is an intermediate case. The cause of the severe distortion in $\hat{\underline{C}}$ at low solar phase angles for the other 12 profiles is evident from Fig. 3, which plots $\underline{v}(\phi,n)$ and shows that for odd n, $\underline{v} \to 0$ as $\phi \to 0$. Since the basic Eq. (1) for calculating $\hat{\underline{C}}$ is $\underline{d}_n = \underline{c}_n/\underline{v}_n$, estimation of odd harmonics in $\hat{\underline{C}}$ becomes increasingly sensitive to lightcurve noise and computational precision as $\phi \to 0$. These simulations and those presented in Section V suggest that reliable determination of odd harmonics is difficult if $|\phi|$ is less than about 5°, and we will not try to estimate $\underline{C}$ from lightcurves taken that close to opposition. Instead, we will use equatorial lightcurves obtained near opposition to estimate $\underline{C}_s$.

As discussed earlier, $\underline{C}_s$ has the same even harmonics as $\underline{C}$ but no odd harmonics. $\underline{C}_s$ actually tells us quite a bit about $\underline{C}$ because the breadth function of any convex profile is independent of the profile's odd harmonics. That is, $\underline{C}_s$ and $\underline{C}$ have the same breadth function because they have the same even harmonics. It is important to note that *at opposition, under the pertinent ideal conditions (EVIG and GEO), an asteroid's lightcurve equals the breadth function of* $\underline{C}_s$ *(and of* $\underline{C}$*) within a multiplicative constant.* Furthermore, $\beta^* = 10^{0.4\Delta m}$, so the lightcurve's amplitude is a trivial function of β^* and thus is a valid gauge of elongation. We stress that this elongation or any other shape-related parameter obtained from a lightcurve pertains *not* to the asteroid's three-dimensional shape but to a two-dimensional *average* of that shape.

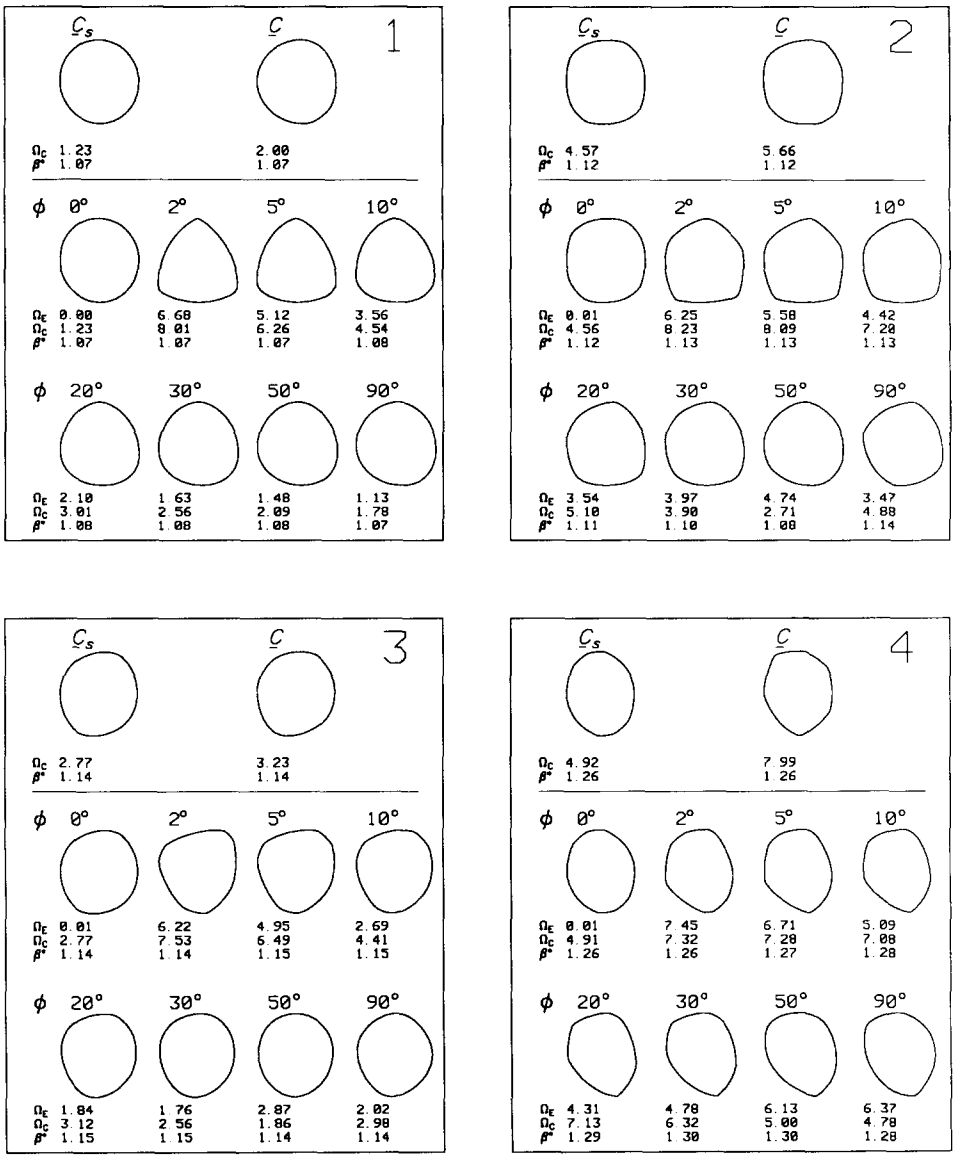

FIG. 6. Effects of nongeometric scattering on estimation of $\underline{C}$ and $\underline{C}_S$. Each box shows results of simulations for a particular model "asteroid." The model's mean cross section and symmetrized mean cross section are shown above the horizontal bar. Below the bar are estimates of those quantities from inversion of lightcurves generated at various solar phase angles ϕ and employing the Hapke photometric function described in the text. ($\hat{\underline{C}}_S$ is estimated at opposition and $\hat{\underline{C}}$ is estimated at the seven nonzero values of ϕ.) Each profile's noncircularity Ω_C and breadth ratio β^* are given. Ω_E is the distance between $\hat{\underline{C}}$ and $\underline{C}$ or between $\hat{\underline{C}}_S$ and $\underline{C}_S$.

For phase angles larger than 5°, convex-profile inversion is increasingly "stable" with respect to estimation of $\underline{C}$'s odd harmonics, but the scattering becomes distinctly nongeometric as $|\phi|$ increases, thereby causing distortion in $\hat{\underline{C}}$. For phase angles equal to 10°, 20°, 30°, and 50°, the average value of Ω_E is 4.1, 3.8, 4.3, and 4.7,

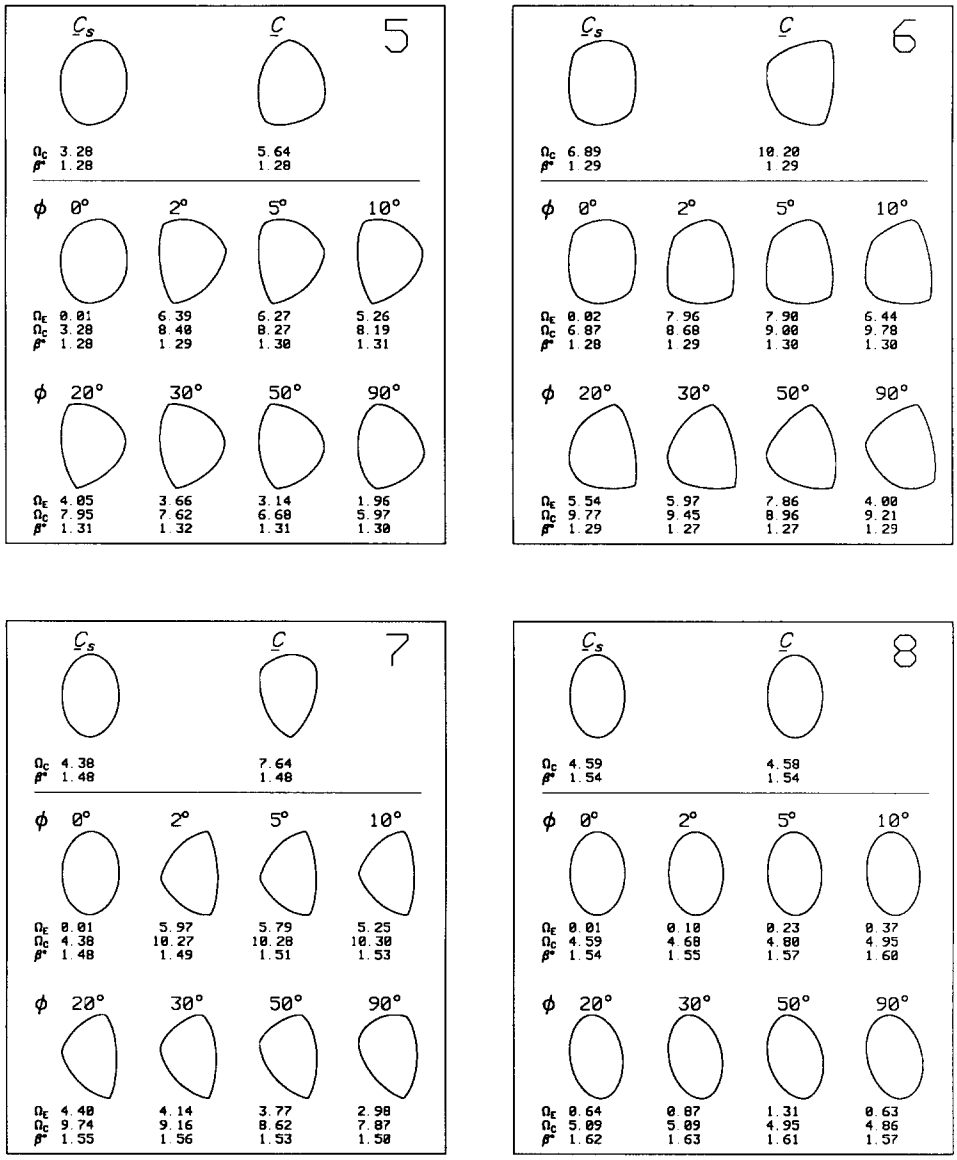

FIG. 6—*Continued.*

with an rms dispersion within 10% of 2.0 throughout. Thus, the systematic error in $\hat{\underline{C}}$ from violation of Condition GEO tends to "bottom out" around 20°, a fortuitous circumstance in view of the inaccessibility of main-belt asteroid lightcurves at much larger solar phase angles.

Our simulations indicate that even for ϕ near 20°, an estimate of $\underline{C}$ is likely to contain some systematic error. Figures 6 and 7 suggest that the distortion in $\hat{\underline{C}}$ can be expected to be moderate for most cases, but negligible for some small fraction of cases and intolerably severe for a comparable fraction. On the other hand, Fig. 8 shows that for ϕ at least as large as 20° the noncircularity is within about ± 1 unit of the asteroid's actual value and that values of β^*

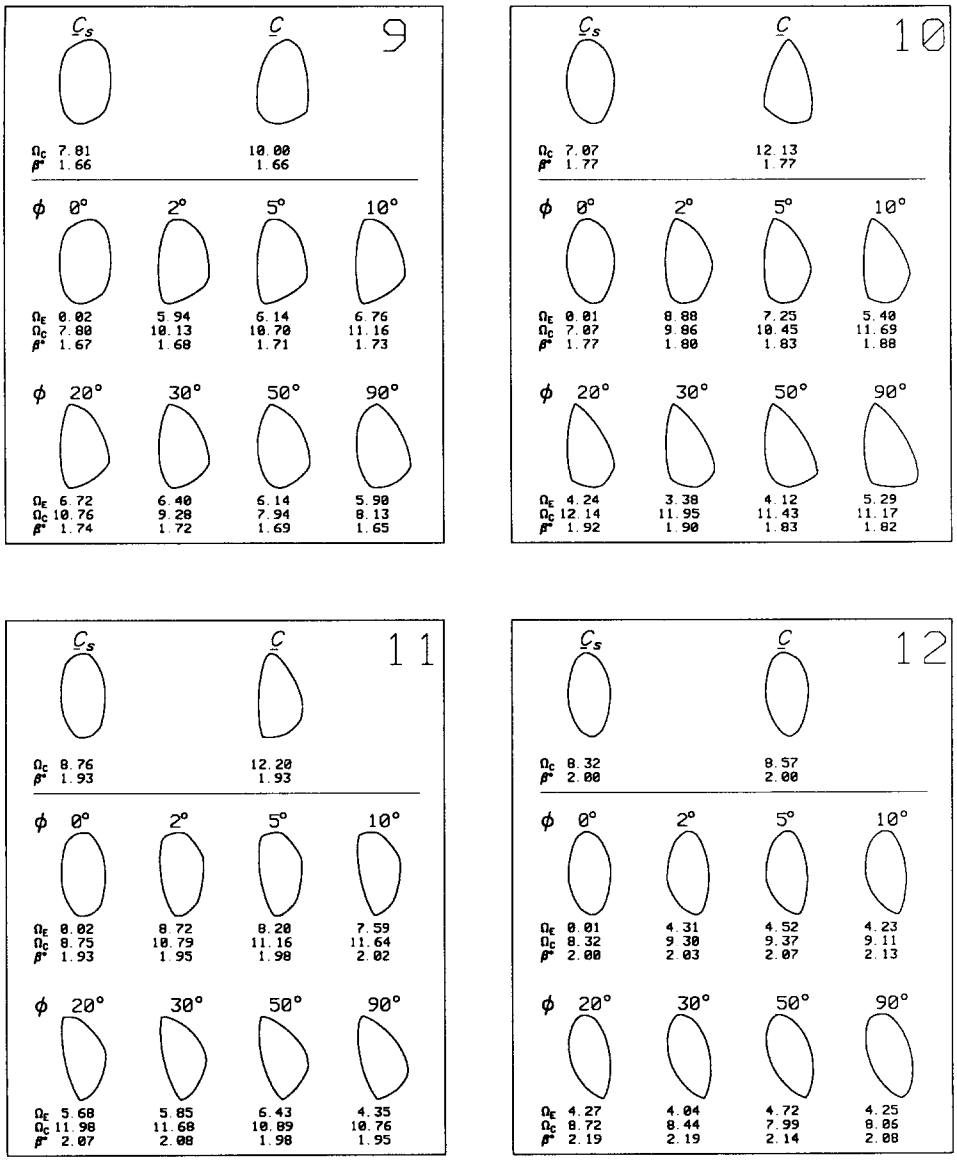

FIG. 6—*Continued.*

estimated for $\hat{\underline{\hat{C}}}$ are within 5% of $\underline{C}$'s value of β^* for all solar phase angles. That is, the salient characteristics of the mean cross section are determined fairly accurately, even when a realistic scattering law is assumed.

Figure 8 also plots the ratio $10^{0.4\Delta m}/\beta^*$, where $10^{0.4\Delta m}$ is the estimate of β^* provided by the lightcurve amplitude. Within about 10° of opposition, the lightcurve amplitude provides a reliable estimator for the elongation of $\underline{C}$, but overestimates the elongation by several tens of percent for ϕ as large as 20°, by factors of several at $\phi = 50°$, and by factors of up to 10 at $\phi = 90°$. It seems clear that a value of β^* derived from $\hat{\underline{\hat{C}}}$ is a gauge of $\underline{C}$'s elongation that not only is more reliable and more physically meaningful than

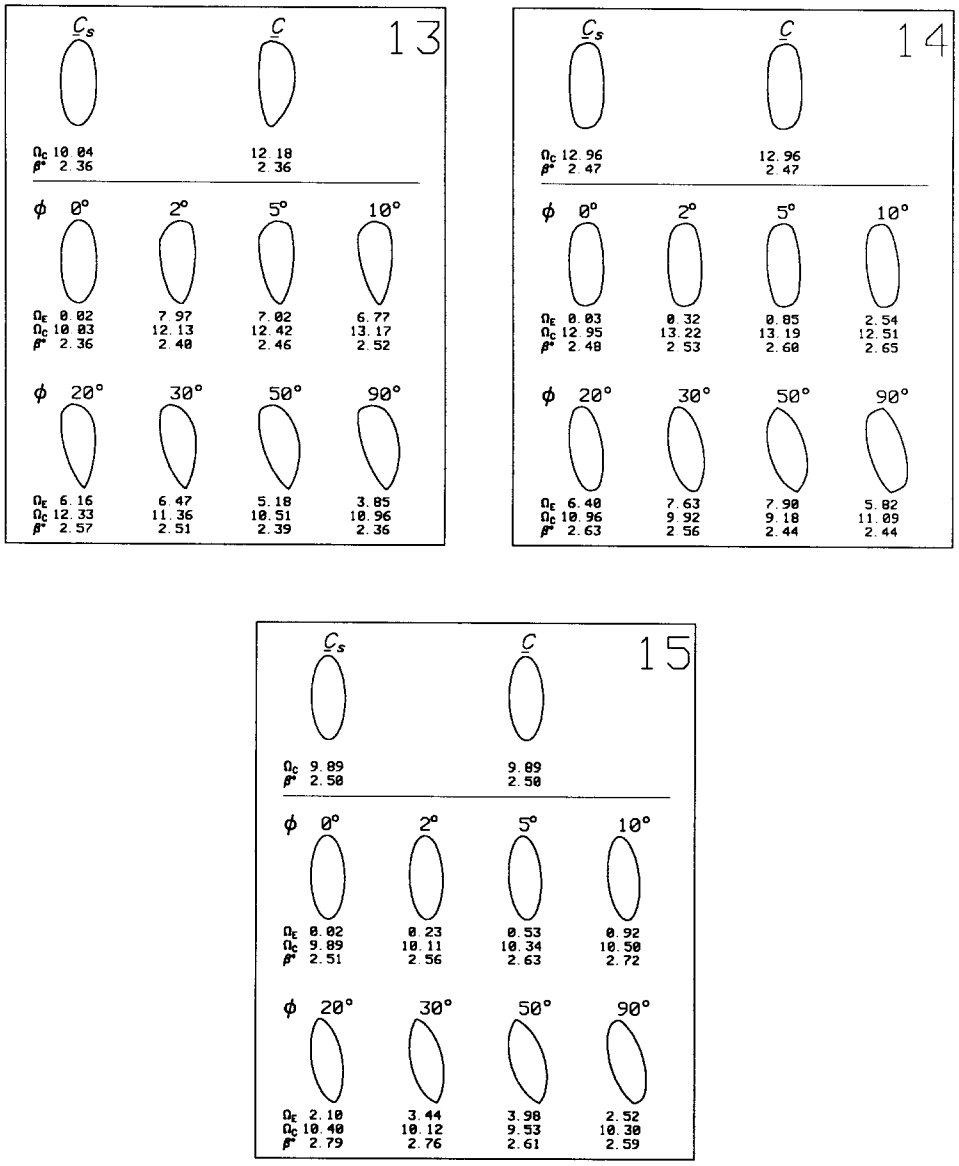

FIG. 6—*Continued.*

Δm, but also compensates for the so-called phase-magnitude relation.

We have not tried to model lightcurves for three-dimensional objects for which $\underline{C}(z)$ is not constant. For any arbitrary shape, $\hat{\underline{C}}$ can be thought of as the sum of potentially distorted versions of the individual $\underline{C}(z)$, where the distortion depends on the local surface curvature and scattering properties at each point. Our simulations have used a realistic approach to scattering properties but have ignored components of curvature that are not parallel to the equator. Hence our results are generally valid only to the extent that the curvature of surface contours not parallel to the equator is irrelevant to distortion in $\hat{\underline{C}}$. In simpler language, we have ignored effects of polar

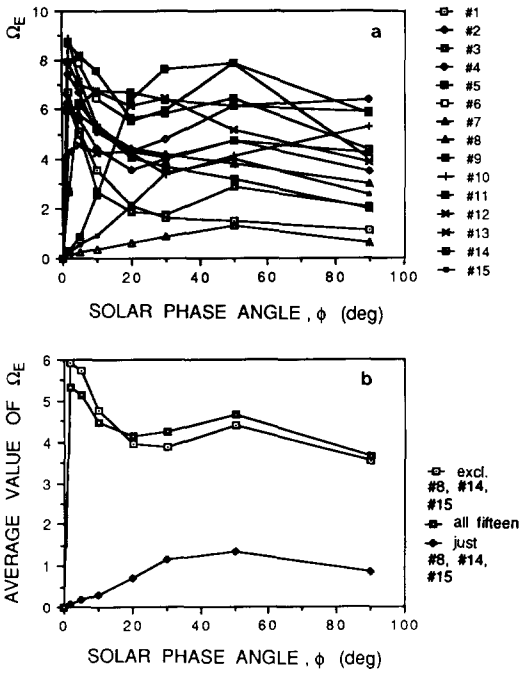

FIG. 7. (a) Individual values of Ω_E for the 15 model asteroids in the simulations described in the text, and (b) average values of Ω_E for three subsets of the model asteroids.

darkening on the functional form of lightcurves. Nevertheless, we suggest that our simulations with constant-$\underline{C}(z)$ shapes may apply to physically realistic convex shapes if Condition EVIG is satisfied, because the weighting of the $\underline{C}(z)$ is such [Ostro and Connelly 1984, Eq. (7) and Appendix A] that contributions to the mean cross section from equatorial $\underline{C}(z)$ can easily dominate those from polar regions. This situation will be even more pronounced for a Hapke scatterer than for a geometric scatterer.

C. *Violation of Condition CONVEX*

We have already dealt with this source of systematic error in a *de facto* sense, because Hapke's theory includes effects of roughness at scales much larger than the observing wavelength. In other words, bias in $\hat{\underline{C}}$ due to concavities is indistinguishable, either *a priori* or *a posteriori,* from bias due to nongeometric (or even nonuniform) scattering. Partially because asteroidal values of $\bar{\theta}$ are unavailable, we have not explored the dependence of Ω_E on $\bar{\theta}$, but such a study might be worth pursuing in the future.

V. PROPAGATION OF LIGHTCURVE ERROR

So far, we have focused on systematic distortion in $\hat{\underline{C}}$ caused by departure from ideal conditions. Since actual lightcurves

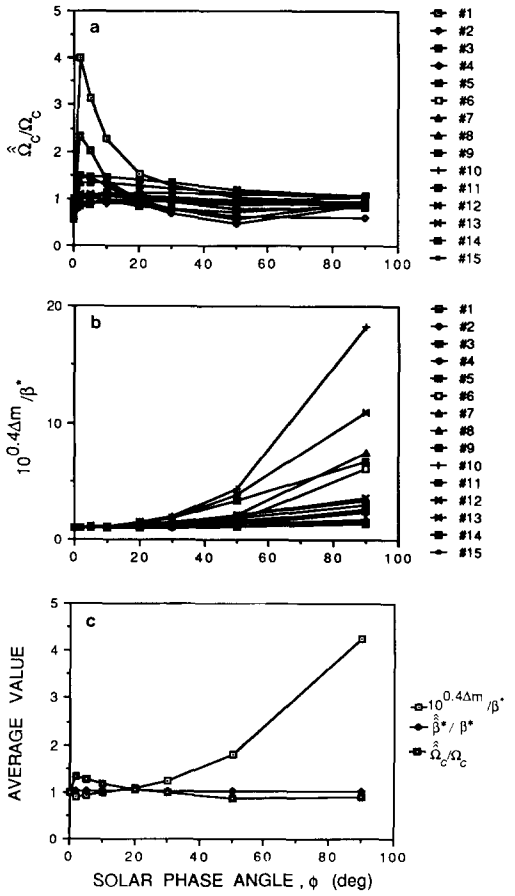

FIG. 8. Estimated values of breadth ratio β^* and noncircularity Ω_C for the simulations described in the text, normalized to the model asteroids' true values. (a) and (b) show individual values for the 15 objects, while (c) plots average values. $\hat{\Omega}_C$ and $\hat{\beta}^*$ correspond to $\hat{\underline{C}}$. $10^{0.4\Delta m}$ is the ratio of the asteroid's maximum brightness to its minimum brightness, i.e., an estimate of β^* derived from the lightcurve amplitude Δm. Individual values of $\hat{\beta}^*/\beta^*$, not shown here, are within 5% of unity for all 15 model asteroids, regardless of solar phase angle.

are contaminated with measurement errors, any estimate of $\underline{C}$ or $\underline{C}_s$ will also contain some statistical error. Whereas actual lightcurve measurement errors may arise from systematic sources (e.g., imperfect removal of sky background, intermittent cirrus, etc.), as well as from photon-counting stochastic errors, one can always compute an "effective standard deviation" in the overall noise due to all sources. Distortion caused by any given noise level will increase as the rotational-phase sampling interval increases.

We have investigated the effects of noise and sampling rate for five of the model asteroids (objects No. 1, 4, 8, 11, and 15) used in Section IV.B. As shown in Fig. 4, those five shapes span a large region in "Ω_c vs β^* space." Here, to focus on statistical sources of error, we assume that all ideal conditions are satisfied. Propagation of statistical error has been modeled by generating a lightcurve for a given model asteroid, using a random number generator to produce Gaussian noise samples, scaling the standard deviation to some fraction σ of the asteroid's mean brightness, adding the scaled noise to the lightcurve, and then estimating $\hat{\underline{C}}$ or $\hat{\underline{C}}_s$. The entire procedure is repeated to build up an ensemble of five profiles, each containing error introduced by a different realization of the same noise-generating random process. We repeated this exercise for two noise levels (σ = 1 and 3%), two sampling intervals ($\Delta\theta$ = 3° and 9°), and four solar phase angles (ϕ = 0°, 5°, 10°, and 20°), for each of the five model asteroids. Our choices of noise level and sampling interval span the values corresponding to many published asteroid lightcurves and let one gauge the severity of statistical error sources in the inversions to be presented in Section V.

Figure 9 superposes the five estimates of $\underline{C}$ for each choice of the three parameters (σ, $\Delta\theta$, ϕ) and also lists the five-profile mean values of the error distance Ω_E, the noncircularity Ω_C, and the breadth ratio β^*, using the same format as in Fig. 6. Note the trade-offs between noise level and sampling rate, and the dependence of Ω_E on solar phase angle. Tripling the noise level generally increases the error distance more dramatically than does tripling the sampling interval, but there is some coupling between σ and $\Delta\theta$, with the negative effect of increasing $\Delta\theta$ felt more severely at the high noise level than at the low noise level.

The accuracy of $\hat{\underline{C}}$ increases with increasing solar phase angle because noise "masquerading" as odd-harmonic energy in a low-ϕ lightcurve gets "blown up" via Eq. (1) into very strong odd harmonics in $\hat{\underline{C}}$. It should not surprise us that reliable estimation of $\underline{C}$'s odd harmonics is intrinsically difficult at low solar phase angles; recall that under the ideal conditions, the manifestation of $\underline{C}$'s odd harmonics as odd harmonics in the lightcurve is *nil* at opposition and grows slowly with $|\phi|$. (See Fig. 3 and Section III.) Note that overestimation of $\underline{C}$'s noncircularity appears correlated with the error distance for the more symmetric shapes, but that the noncircularity is fairly immune to noise for the shapes (objects No. 4 and 11) containing healthy odd harmonics.

Estimation of the symmetrized mean cross section (i.e., of $\underline{C}$'s even harmonics) is accurate even for the higher noise level and coarser sampling interval. This situation reflects the intrinsic accessibility of $\underline{C}$'s even harmonics, regardless of ϕ. Consequently, β^*, whose value depends only on $\underline{C}$'s even harmonics, is estimated quite reliably for every one of our simulations.

Since systematic sources of error in $\hat{\underline{C}}$ can be severe, it is important that statistical sources of error be minimized for lightcurves acquired to constrain asteroid shapes. A conservative rule of thumb might be to try to keep σ at or below ~1%. At that level, statistical sources of error in $\hat{\underline{C}}$ seem small compared to distortion introduced by violation of Conditions EVIG and/or GEO. (In the following section, we apply convex-profile inversion to lightcurves whose noise levels range from 0.6 to 4% and average

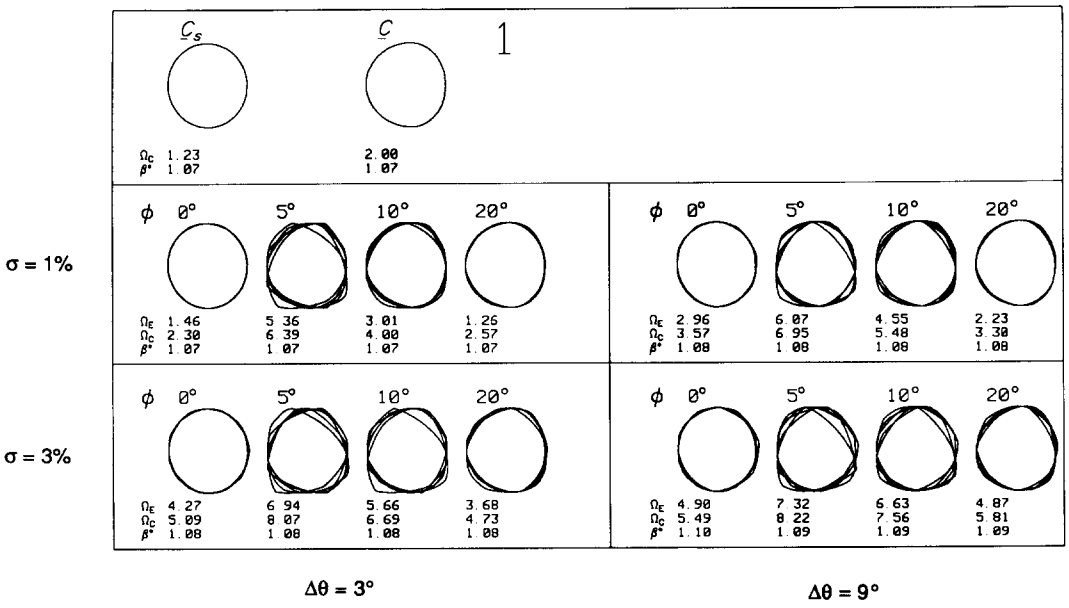

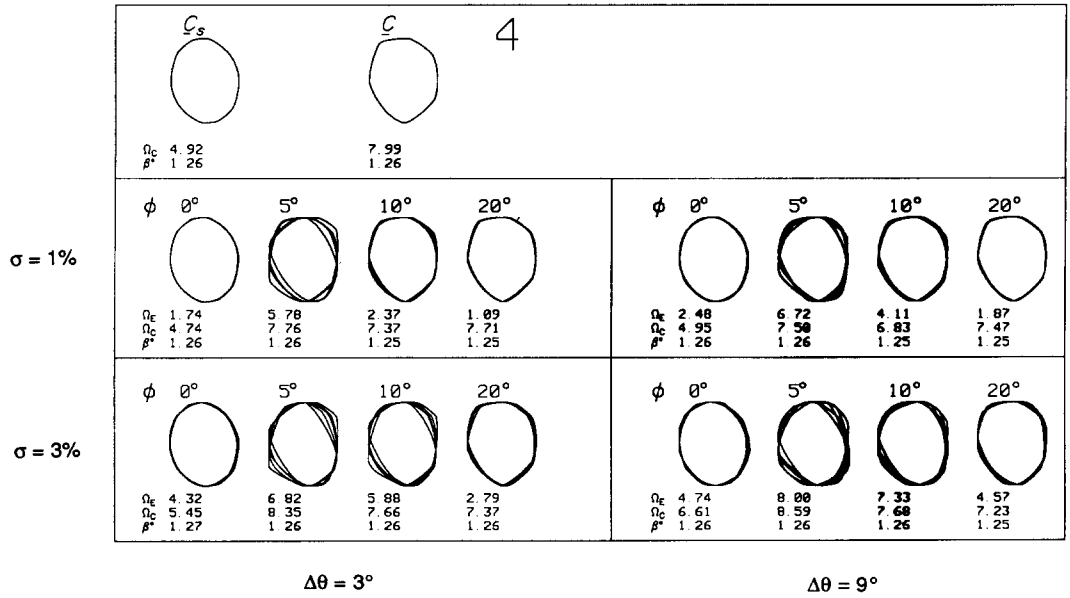

FIG. 9. Propagation of statistical error for five model asteroids. This figure is in the same format as Fig. 6. Each box shows results of simulations for a particular model. The model's mean cross section and symmetrized mean cross section are shown above the horizontal bar. Below the bar are estimates of those quantities from inversion of noisy lightcurves generated under ideal conditions at solar phase angle ϕ, noise level σ, and rotational-phase sampling interval $\Delta\theta$. ($\hat{\underline{C}}_s$ is estimated at opposition and $\hat{\underline{C}}$ is estimated at the three nonzero values of ϕ.) Five cross section estimates, corresponding to five different realizations of the noise-generating random process, are superposed for each choice of ϕ, σ, $\Delta\theta$. Five-profile mean values of noncircularity Ω_C, breadth ratio β^*, and error distance Ω_E are listed. See text.

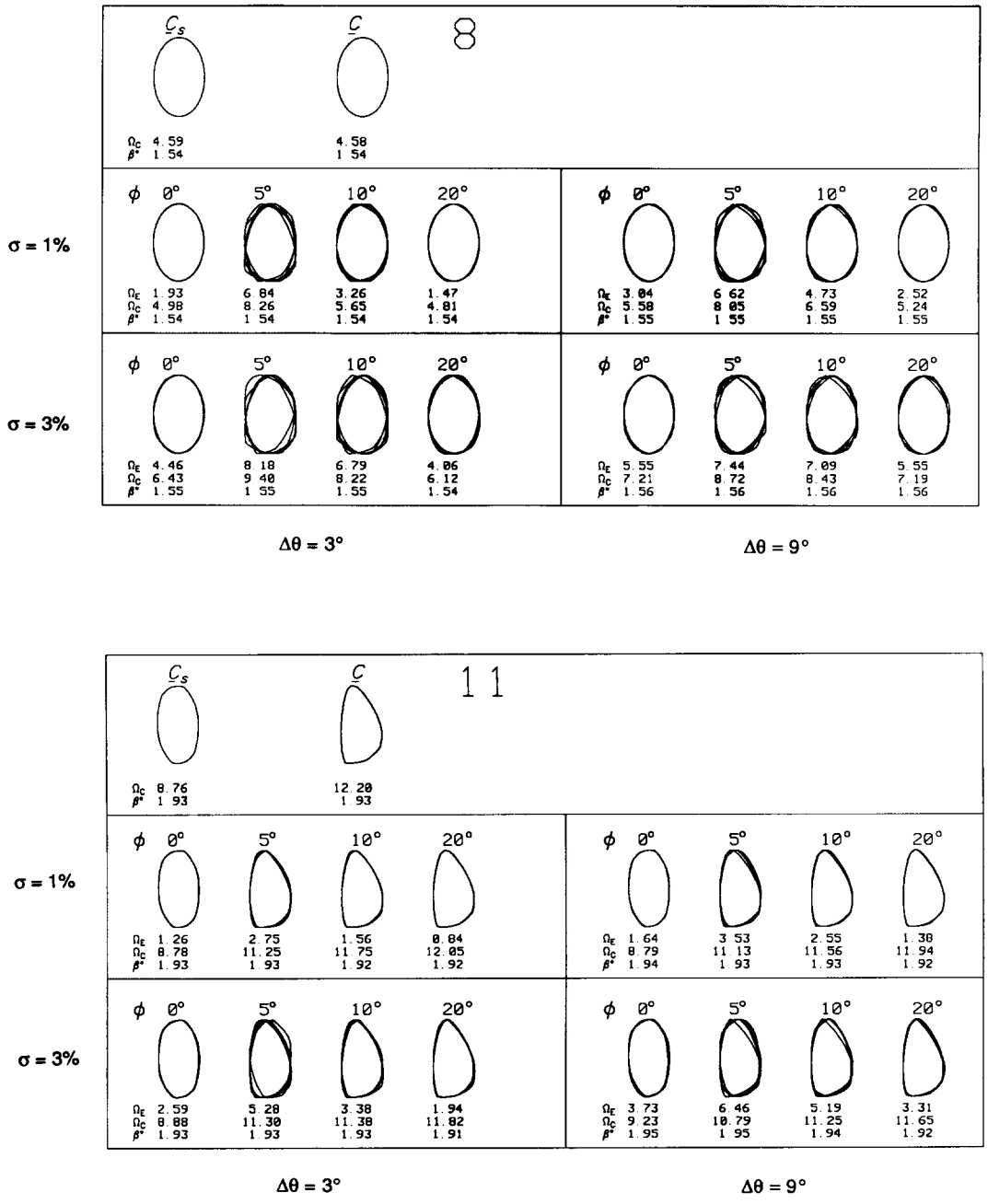

FIG. 9—*Continued.*

~1.5%. Our simulations suggest that for such noise levels, statistical error in an estimate of the breadth ratio will not exceed a few percent of β^*, while that in an estimate of the noncircularity will typically be about 1 distance unit or less. The bias in an estimate of β^* will usually be negligible, but the bias in an estimate of $\underline{C}$'s Ω_c obtained at low solar phase angle can be several distance units at the higher noise levels.)

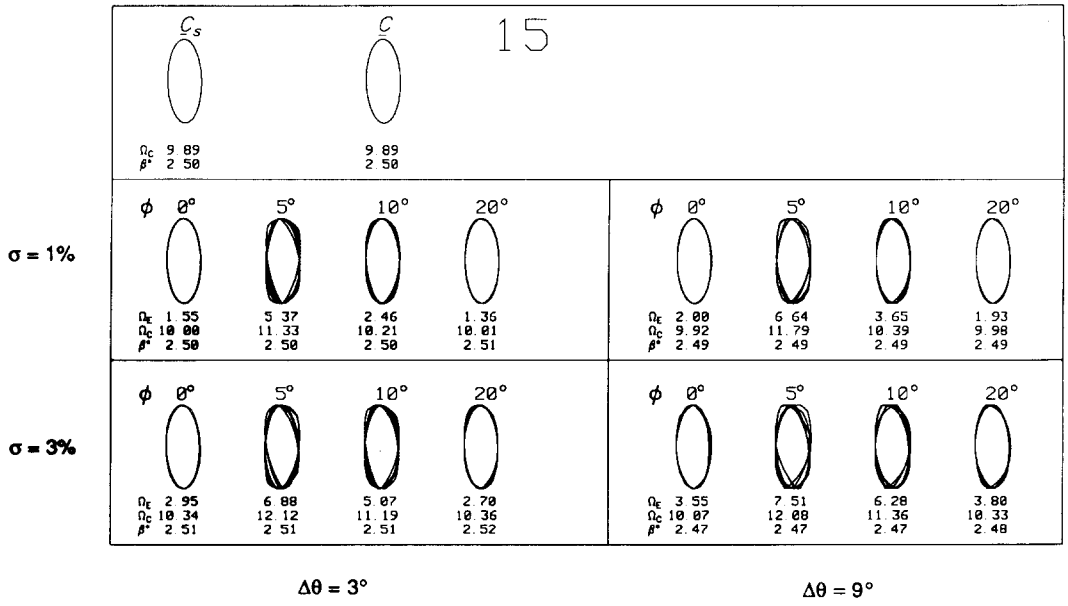

FIG. 9—*Continued.*

The sampling interval is less critical, especially at low noise levels and large solar phase angles. However, simulations not presented here indicate that gaps in rotational-phase coverage as large as a few tens of degrees can increase Ω_E by several tens of percent. For this reason, it seems prudent to interpret the parameter $\Delta\theta$ in the Fig. 9 simulations as the *minimum* interval between any two data points.

VI. APPLICATIONS

In this section, we present results of applying convex-profile inversion to selected asteroids, beginning with lightcurves for which prior knowledge of the asteroid's pole direction indicates viewing-illumination geometry not far from equatorial. Note that for all lightcurves shown below, we plot the brightness in *linear* units scaled so that the average brightness is near unity; accordingly, we express Δm in linear units instead of magnitudes.

To help guide interpretation of our results, each of the figures referred to in this section includes values for several goodness-of-fit statistics. If the ideal conditions were satisfied perfectly, then the (unconstrained) Fourier model $\hat{\mathbf{y}}$ for the lightcurve data $\mathbf{y}$ would be the same as the (constrained) Fourier model $\hat{\hat{\mathbf{y}}}$ corresponding to $\hat{\underline{C}}$. (See Section III.) Ostro and Connelly (1984) describe a test of the null hypothesis, H_0, that the vector of Fourier coefficients for $\hat{\hat{\mathbf{y}}}$ is a statistically acceptable estimate of the Fourier vector for the "true" lightcurve. This "variance ratio" test compares an estimate of σ^2 obtained from the residuals between the data and $\hat{\hat{\mathbf{y}}}$ to an estimate obtained from the residuals between the data and $\hat{\mathbf{y}}$. Let M be the number of Fourier harmonics and L the number of data points, and let us assume that the errors in $\mathbf{y}$ are independent, identically distributed, zero-mean, Gaussian random variables. Then the following goodness-of-fit statistic, w_1, is distributed as $F_{\nu_1,\nu_2,\alpha}$ under the null hypothesis (Plackett 1960, p. 52 ff.):

$$w_1 = (R - 1)\nu_1/\nu_2$$

where

$$R = (\mathbf{y} - \hat{\mathbf{y}})^{\mathrm{T}}(\mathbf{y} - \hat{\mathbf{y}})/(\mathbf{y} - \hat{\mathbf{y}})^{\mathrm{T}}(\mathbf{y} - \hat{\mathbf{y}})$$

$$\nu_1 = 2M + 1$$

$$\nu_2 = L - \nu_1.$$

We can reject H_0 at the $100(1 - \alpha)\%$ confidence level whenever $w_1 > F_{\nu_1,\nu_2,\alpha}$. For example, H_0 can be rejected at the 99% confidence level if $w_1 > F_{\nu_1,\nu_2,0.01}$. For all inversions in this paper, $M = 10$, $L > 45$, and $F_{\nu_1,\nu_2,0.01} < 3$.

In the figures below, we give up to three goodness-of-fit statistics for each inversion. The first, w_1, tests H_0 for $\hat{\mathbf{y}}$, as just described; if w_1 exceeds 3, we can safely reject H_0. The second, w_2, tests the same hypothesis, but for the lightcurve model $\hat{\mathbf{y}}_S$ corresponding to $\underline{\hat{C}}_S$. The third, w_3, tests the same hypothesis as w_2, but assumes that the correct lightcurve model is $\hat{\mathbf{y}}$, instead of $\hat{\mathbf{y}}$ as for w_1 and w_2. If the third w statistic is ≥ 3, then we can safely reject the hypothesis that $\underline{\hat{C}}_S$ provides as good a fit to the lightcurve data as does $\underline{C}$. Whenever we estimate $\underline{\hat{C}}$, we also give the "symmetrization distance" Ω_S between $\underline{\hat{C}}$ and $\underline{\hat{C}}_S$.

A. *Objects with Published Pole Directions*

15 Eunomia. Figure 10 shows $\underline{\hat{C}}$ (solid profile) and $\underline{\hat{C}}_S$ (dotted profile) estimated from lightcurves at solar phase angles equal to $-12°$ and $-21°$. The signs of ϕ assume retrograde rotation, as deduced by authors cited in the figure caption. Using Magnusson's (1986) values for the ecliptic longitude ($106° \pm 5°$) and latitude ($-73° \pm 10°$) of Eunomia's north pole, we calculate (δ_E, δ_S) equal to (19°, 18°) and (8°, −2°) for the two Eunomia curves.

The figure shows that the values of the elongation β^* and the noncircularity Ω_C for the two estimates of $\underline{C}$ vary by less than 10%. If the ideal conditions held perfectly and if the lightcurves were free of noise, then $\underline{\hat{C}}$ and those two shape descriptors would be independent of solar phase angle. The ideal conditions certainly are not satisfied perfectly and the lightcurves are not noiseless, but the similarity of the profiles obtained from the two lightcurves lends confidence to their validity and is consistent with the *net* effect of the violations of the ideal conditions being fairly small. Also note that the fractional variation in the estimates of β^* (which pertains to the asteroid's mean cross section) is half that in the estimates of Δm (which pertains to the lightcurves); see the discussion in Section IV.B.

The fact that the values of w_1 and w_2 exceed 3 is interpretable as very strong evidence for violation of ideal conditions. However, caution is advised even when those statistics are near unity, since violations of ideal conditions might conspire to produce a lightcurve yielding a good match between $\hat{\mathbf{y}}$ and the lightcurve data, but a $\underline{\hat{C}}$ that nevertheless is inaccurate. By the same token, it is conceivable that a mean cross section estimate providing a poor fit to the data might be physically valid. Given these various possibilities, it clearly is desirable to estimate an asteroid's mean cross section at a variety of solar phase angles.

Figure 10 also shows the weighted average of the two estimates of Eunomia's mean cross section, calculated by summing the statistically weighted vector of Fourier coefficients for the radius-of-curvature functions for the individual profiles, with the profiles' relative rotational phase chosen to maximize the cross correlation of the radius-of-curvature functions. This example demonstrates how convex-profile inversion can combine the shape information contained in any number of independent lightcurves, perhaps taken at a variety of solar phase angles and/or during different apparitions.

19 Fortuna. Figure 11 shows $\underline{\hat{C}}$ for two lightcurves obtained by Weidenschilling *et al.* (1987) for 19 Fortuna, and their weighted average. This asteroid's lightcurves have peak-to-valley amplitudes close to 0.25 mag, independent of ecliptic longitude, suggesting that the asteroid-cen-

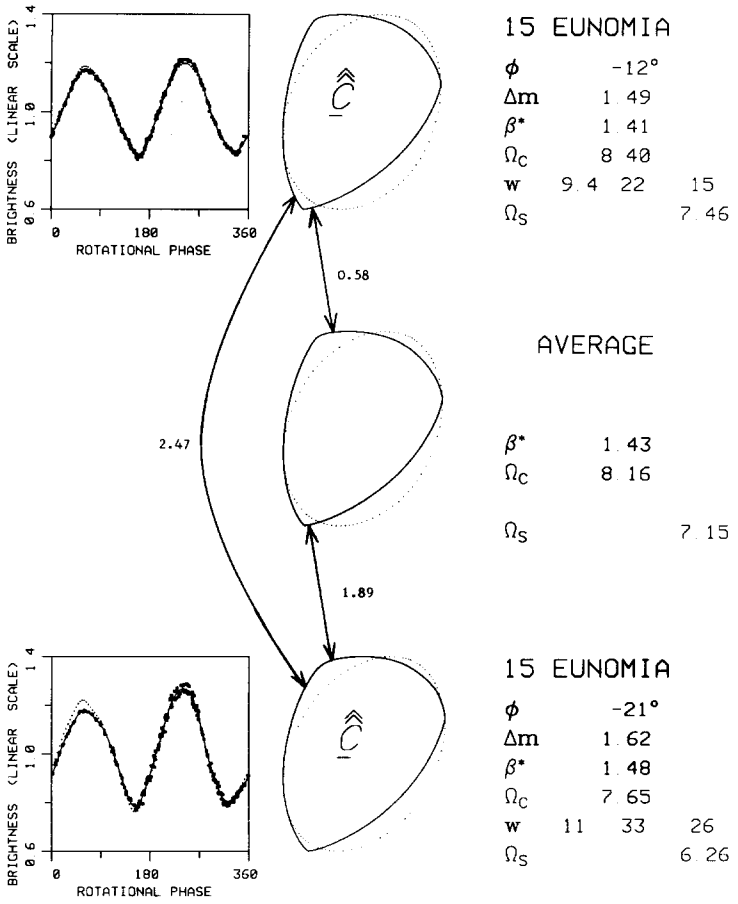

FIG. 10. Estimates of $\underline{C}$ (the solid profile) and $\underline{C}_s$ (the dotted profile) for lightcurves obtained for asteroid 15 Eunomia at solar phase angle $\phi = -12°$ (Fig. 8 of Groeneveld and Kuiper 1954) and at $\phi = -21°$ (Fig. 14 of van Houten-Groeneveld and van Houten 1958). All the lightcurves in this paper are plotted on a *linear* scale, with the average brightness set to unity. In the lightcurve plots, the large symbols are the data, the solid lightcurve $\hat{\mathbf{y}}$ was derived from the unconstrained vector of Fourier coefficients $\hat{\mathbf{x}}$, and the dotted lightcurve $\hat{\mathbf{y}}$ was derived from the constrained Fourier coefficients ($\hat{\mathbf{x}}$) corresponding to $\hat{\underline{C}}$. On the right, Δm is the ratio of $\hat{\mathbf{y}}$'s maximum to its minimum; β^* is the breadth ratio (the same for $\hat{\underline{C}}$ and $\hat{\underline{C}}_s$); Ω_C is the noncircularity of the profile drawn with a solid curve, here $\hat{\underline{C}}$; and Ω_S is the distance between $\hat{\underline{C}}$ and $\hat{\underline{C}}_s$. To the right of "w" are values for three statistics that let us test hypotheses described in the text. Briefly, since the first statistic (w_1) exceeds 3, we can safely state that the lightcurve corresponding to the mean cross section estimate is not a good fit to the data. Since the second statistic (w_2) exceeds 3, we can make the same statement about the symmetrized mean cross section. Since the third statistic (w_3) exceeds 3, we can state that the difference between the lightcurves corresponding to $\hat{\underline{C}}$ and $\hat{\underline{C}}_s$ is significant, i.e., that the odd harmonics in $\hat{\mathbf{y}}$ are statistically significant. (In some of the subsequent figures we just estimate $\hat{\underline{C}}_s$, and in those we do not give values for Ω_S, w_1, or w_3.) In the middle of this figure are the weighted average of the two individual estimates of $\underline{C}$, its symmetrization, and relevant shape descriptors. Note the distances between the cross section estimates.

tered declinations of Earth and the Sun are within a few tens of degrees of zero.

20 Massalia and 129 Antigone. Figures 12 and 13 show results of inverting an opposition lightcurve and a nonopposition lightcurve for each of these large, main-belt as-

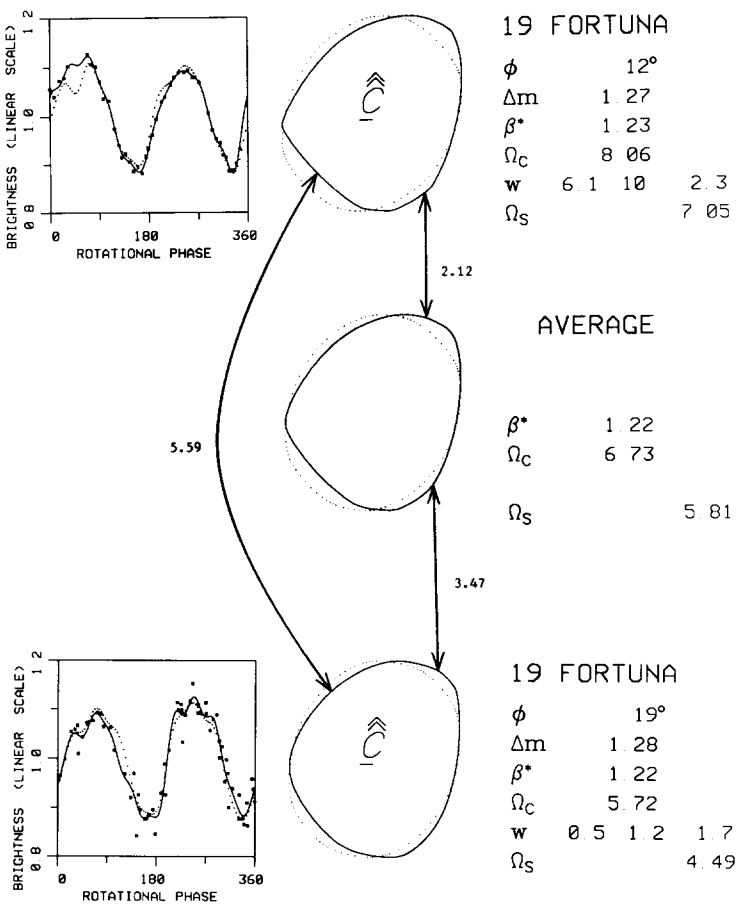

FIG. 11. Similar to Fig. 10, but for lightcurves of asteroid 19 Fortuna obtained by Weidenschilling *et al.* (1987).

teroids. For each object, Magnusson's (1986) pole position estimates are consistent with the asteroid-centered declinations of the Sun and Earth being within a few tens of degrees of zero during the observations.

If an estimate of $\underline{C}$ from a nonopposition lightcurve were accurate, then its symmetrization would provide an estimate of $\underline{C}_s$ that would also be accurate and hence would resemble an estimate of $\underline{C}_s$ from an opposition lightcurve. We expect $\hat{\underline{C}}$ to be more reliably estimated from an opposition lightcurve because the scattering is likely to be closer to geometric at small ϕ.

For Massalia, the two estimates of $\underline{C}_s$ are nearly identical (Ω = 2.33), lending confidence to their mutual validity. The poor goodness of fit for the inversion of the opposition lightcurve is disconcerting, but note that the residuals are spread out fairly uniformly over 360° of rotational phase.

For Antigone, the two estimates of $\underline{C}_s$ are 6.20 distance units apart—they are definitely different—and the residuals are severe, so the cross section estimates are likely to contain significant systematic errors. The presence of a strong first harmonic in the lightcurve taken only 7° from opposition and, if Magnusson's pole direction is correct, at (δ_E, δ_S) equal to (17°, 12°) is interpretable as evidence for a nonuniform albedo distribution.

624 Hektor. Figure 14 shows $\hat{\underline{C}}_s$ esti-

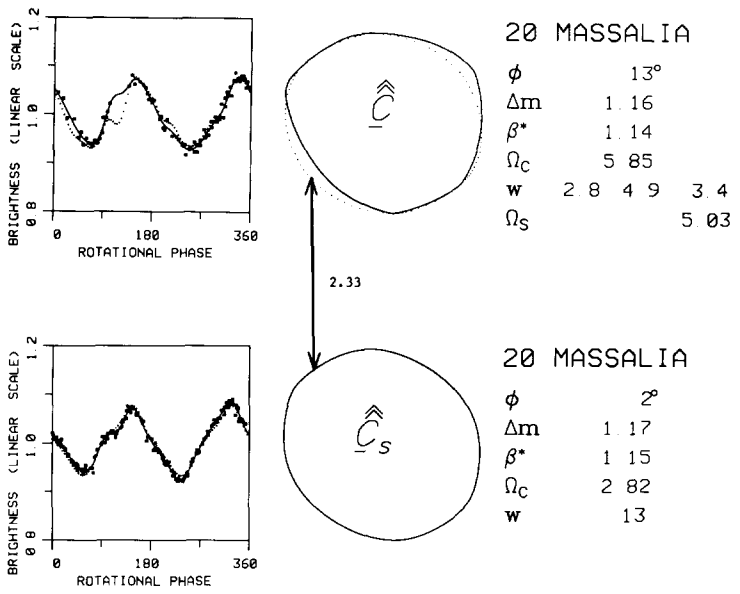

FIG. 12. Inversion of lightcurves obtained for 20 Massalia by Gehrels (1956, composite of his Figs. 4 and 5) at $\phi = 13°$ and by Barucci *et al.* (1985) at $\phi = 2°$. Note the resemblance between the symmetrization (dotted profile) of our estimate of $\underline{C}$ from the nonopposition lightcurve and the estimate of $\underline{C}_s$ from the opposition lightcurve. See Fig. 10 caption.

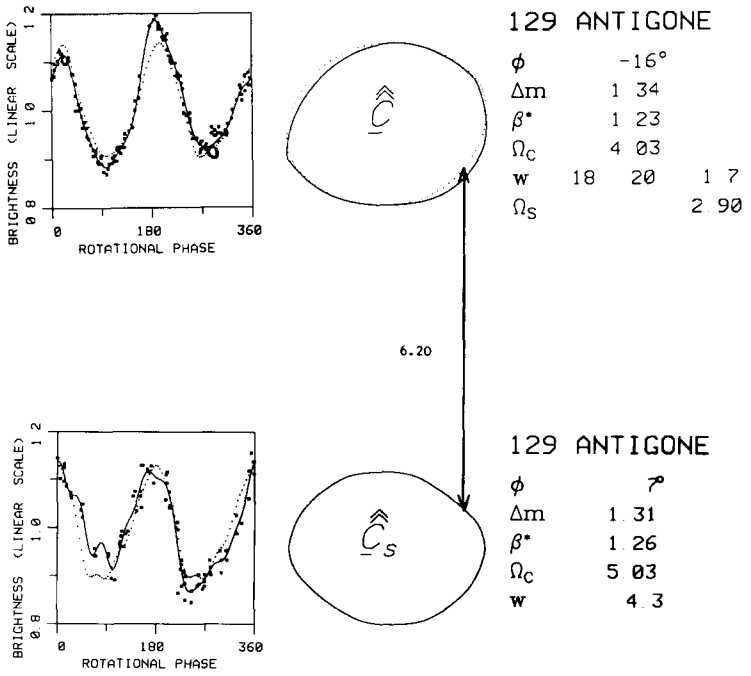

FIG. 13. Convex-profile inversion of lightcurves of asteroid 129 Antigone obtained by Barucci *et al.* (1985) at $\phi = 7°$ and by Scaltriti and Zappalà (1977) at $\phi = -16°$. See Fig. 10 caption, Fig. 12, and text.

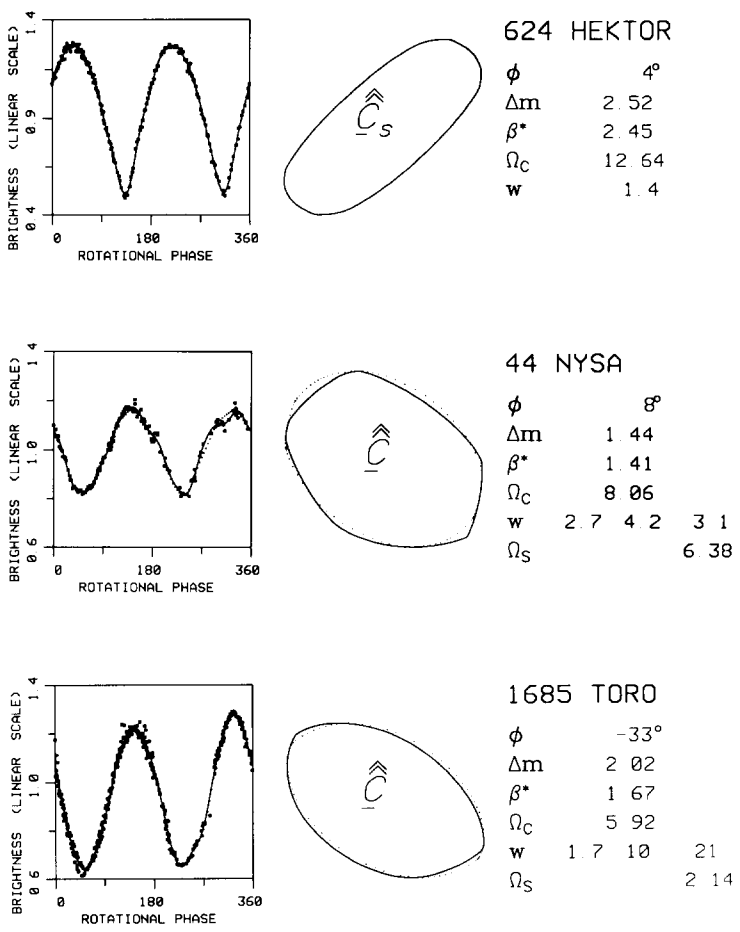

FIG. 14. *Top:* Estimate of the symmetrized mean cross section of asteroid 624 Hektor for a near-opposition lightcurve obtained by Dunlap and Gehrels (1969). *Middle:* Estimation of 44 Nysa's symmetrized mean cross section from a lightcurve obtained by di Martino *et al.* (1987). *Bottom:* Estimates of $\underline{C}$ and $\underline{C}_s$ for 1685 Toro, from inversion of a lightcurve obtained by Dunlap *et al.* (1973). See text and Fig. 10 caption.

mated for 624 Hektor from a lightcurve obtained at $\phi = 4°$ by Dunlap and Gehrels (1969). The pole directions estimated for this Trojan asteroid by those authors (and more recently by Zappalà and Knežević 1984, Pospieszalska-Surdej and Surdej 1985, Magnusson 1986) indicate that δ_E and δ_S have absolute values less than 10°. The constancy of Hektor's color indices with rotational phase (Dunlap and Gehrels 1969), the absence of odd harmonics in the lightcurve, and the low value of w_2 concur in supporting the reliability of our estimate of $\underline{C}_s$. Note that the profile has $\beta^* = 2.5$ and is distinctly nonelliptical. Since the mean cross section of an ellipsoid rotating about a principal axis is an ellipse, our results suggest that neither the asteroid nor its convex hull are ellipsoids. On the other hand, our $\hat{\underline{C}}$ is quite consistent with many other models for Hektor's three-dimensional shape, including a cylinder with rounded ends (Dunlap and Gehrels 1969), a dumbbell (Hartmann and Cruikshank 1978), and various binary configurations (Weidenschilling 1980). Of course, in making these state-

ments, we ignore effects of possible small violations of the ideal conditions.

44 Nysa. As noted by di Martino *et al.* (1987) and Magnusson (1986), this asteroid's pole is relatively well known. The inverted lightcurve (middle row of Fig. 14), from di Martino *et al.* (1987), was taken at a solar phase angle of 8.5°, under nearly equatorial viewing/illumination geometry. The pole estimate yields $\delta_E = 9°$ and $\delta_S = 3°$, so the longitudinal separation of the sub-Earth and sub-Sun points is only about 5°, and our "leverage" in estimating $\underline{C}$'s odd harmonics is marginal at best. On the other hand, our estimate of $\underline{C}_S$ probably is reliable. It is interesting that our estimate, $\beta^* = 1.41$, for the elongation of Nysa's mean cross section is within several percent of values derived for a model ellipsoid's equatorial axis ratio from analysis of a multi-apparition lightcurve data set (Pospieszalska-Surdej and Surdej 1985, Magnusson 1986).

1685 Toro. We assumed the pole direction (200°, 55°) quoted by Dunlap *et al.* (1973) in inverting their July 1972 lightcurve data (bottom row of Fig. 14), and the negative sign of ϕ corresponds to direct rotation. The fit is excellent. Note that $\hat{\underline{C}}$ is much less elongated than one might infer from the lightcurve's large amplitude. Also note that whereas $\Omega_S = 2$, so $\hat{\underline{C}}_S$ is not far from $\hat{\underline{C}}$, w_2 and w_3 are each much greater than 3. That is, the lightcurve's odd harmonics are prominent while $\hat{\underline{C}}$'s are not. There is no discrepancy here; odd harmonics in shape generate increasingly large odd harmonics in a lightcurve as the solar phase angle increases. [See (1) and Fig. 3.]

B. Objects with Unknown Pole Directions

Figure 15 shows $\hat{\underline{C}}$ and/or $\hat{\underline{C}}_S$ for objects for which pole-direction estimates are lacking. We present these profiles because the goodness-of-fit statistics are small, or in some cases because the profiles are interesting, or simply to illustrate the mapping from lightcurve space to profile space, e.g., the relation [Eq. (1) and Fig. 3] between the harmonic structure of a lightcurve and that of a mean-cross-section estimate. Unless otherwise noted, all estimates of $\underline{C}$ assume that ϕ's sign is positive; the profile obtained for a negative sign generally is similar, with nearly the same β^* and Ω_C as the profile shown.

36 Atalante. As di Martino *et al.* (1987) point out, even though this lightcurve's amplitude is similar to that in lightcurves obtained 70° of longitude away, the viewing/illumination geometry might not necessarily be equatorial. The fit is awful (w_1 is huge), with strong, positive residuals for half a cycle but strong negative residuals for the other half. This situation is consistent with a hemispheric albedo asymmetry, so perhaps this object should be targeted for polarimetry or multicolor photometry.

60 Echo. The fit of the model lightcurve corresponding to $\hat{\underline{C}}_S$ to Zeigler and Florence's (1985) data is okay, with no major residuals except at the primary maximum.

61 Danae. To the best of our knowledge, this object has not been observed photometrically since Wood and Kuiper (1963) acquired this lightcurve. At such a small solar phase angle a mean cross section estimate is probably unreliable, and we show $\hat{\underline{C}}$ primarily as an example of a shape with a large noncircularity.

69 Hesperia. The residuals are large, suggesting violation of Condition EVIG and/or Condition GEO. Compare $\hat{\underline{C}}_S$ to Danae's, which has similar values of the shape descriptors β^* and Ω_C.

118 Peitho. This Stanzel and Schober (1980) opposition lightcurve has an unusually strong fourth harmonic, which manifests itself in the rectangular appearance of $\hat{\underline{C}}_S$. The large residuals could be due to albedo heterogeneities and/or to non-equatorial viewing/illumination geometry.

164 Eva. The large value of w_1 is a bit misleading here. The number of points plotted in the Schober (1982) lightcurve is huge, and our digitization of it yielded more than 700. With this many data points the *F*-ratio test becomes extremely sensitive. The

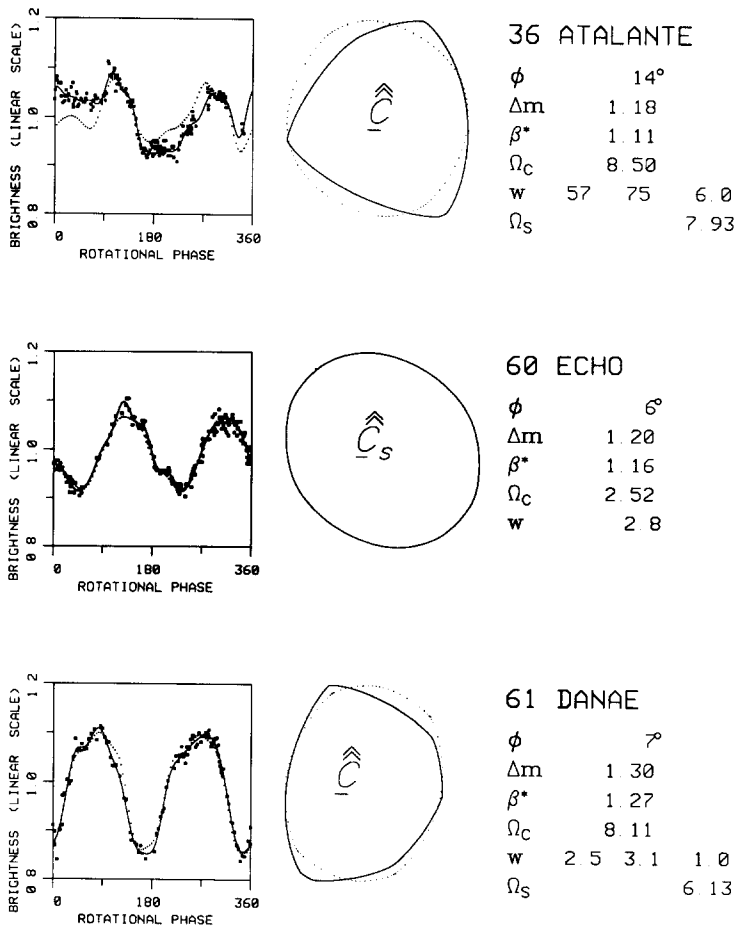

FIG. 15. Estimates of $\underline{C}$ and/or $\underline{C}_s$ for asteroids lacking published estimates of pole direction. See text and Fig. 10 caption. Sources of the lightcurves are 36 Atalante (di Martino *et al.* 1987, Fig. 4), 60 Echo (Zeigler and Florence 1985, Fig. 4), 61 Danae (Wood and Kuiper 1963, Fig. 7), 69 Hesperia (Poutanen *et al.* 1985, Fig. 4), 118 Peitho (Stanzel and Schober 1980, Fig. 1), 164 Eva (Schober 1982, Fig. 3), 246 Asporina (Harris and Young 1983, Fig. 29), 270 Anahita (Harris and Young 1980, Fig. 18), 434 Hungaria (Harris and Young 1983, Fig. 38), 505 Cava (Harris and Young 1985, Fig. 2), 704 Interamnia (Lustig and Hahn 1976, Fig. 11), 739 Mandeville (Zappalà *et al.* 1983, Fig. 28), 1173 Anchises (French 1987), 1627 Ivar (Hahn *et al.* 1987), 2156 Kate (Binzel and Mulholland 1983, Fig. 18).

model lightcurve $\hat{\mathbf{y}}$ corresponding to our mean cross section estimate actually is very slightly lower than the unconstrained model lightcurve $\hat{\mathbf{y}}$ at each of the extrema except the deepest minimum, where it is slightly higher than $\hat{\mathbf{y}}$.

246 Asporina. The Harris and Young (1983) lightcurve has only 65 points, so the *F*-ratio test is not very sensitive to the difference between $\hat{\mathbf{y}}$ and $\hat{\mathbf{y}}$. Contrast with the situation for 164 Eva.

270 Anahita. Differences between the shapes of the two peaks (i.e., odd harmonics in the lightcurve) cause the large value of w_2.

434 Hungaria. Despite the large residuals over rotational phases from 250° to 360°, this inversion demonstrates that, at large

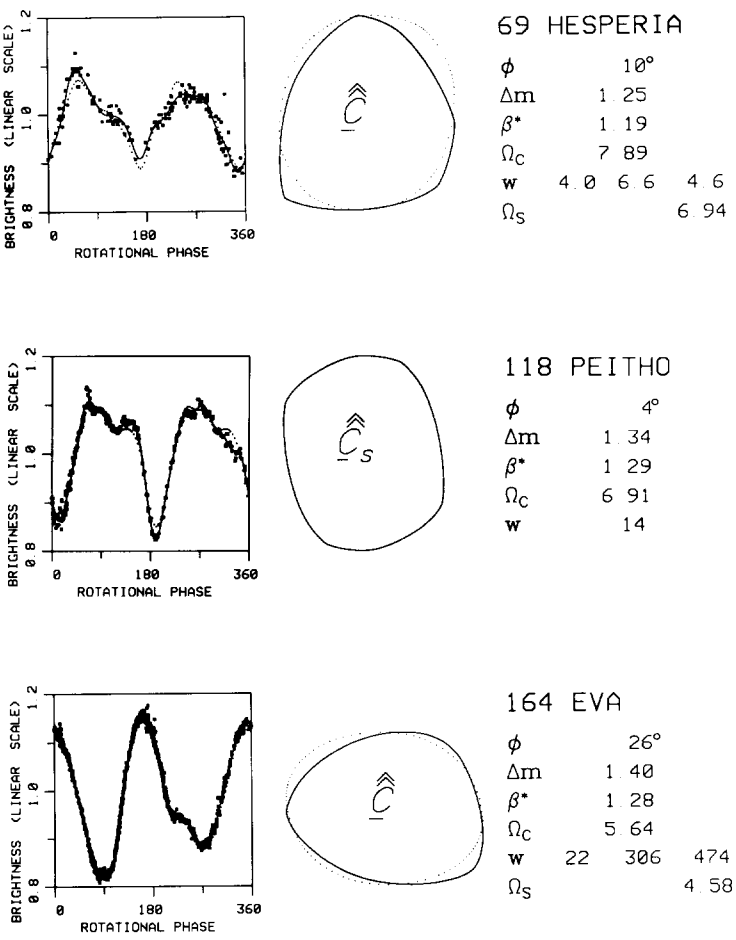

FIG. 15—*Continued.*

solar phase angles, the breadth ratio β^* is superior to Δm as an elongation measure.

505 Cava. The lightcurve from Harris and Young (1985) is composited from data taken at phase angles ranging from 10° to 25°, and we use an average value of 15° for the inversion. The fit of $\hat{\mathbf{y}}$ to the data is good except near $\phi = 270°$; readers might care to speculate about the source of this "feature."

704 Interamnia. The fit of $\hat{\mathbf{y}}$ to the lightcurve obtained by Lustig and Hahn (1976) is not good, but the three pairs of extrema are replicated, and we show this inversion because $\hat{\underline{C}}$ offers a simple explanation for the existence of three minima with different depths: The three pairs of extrema arise because $\hat{\underline{C}}$ resembles an equilateral triangle, while differences between the minima arise because the triangle's vertices have different "sharpnesses."

739 Mandeville. The slightly different shapes of the minima in this Zappalà *et al.* (1983) lightcurve are the source of the odd harmonics in $\hat{\underline{C}}$, which provides a decent fit to the data and, in view of the values of Ω_s and w_3, a significantly better one than does $\hat{\underline{C}}_s$.

1173 Anchises. This opposition lightcurve obtained by French (1987) yields an estimate of $\underline{C}_s$ which is notable for its elongation ($\beta^* = 1.6$) and its interesting shape,

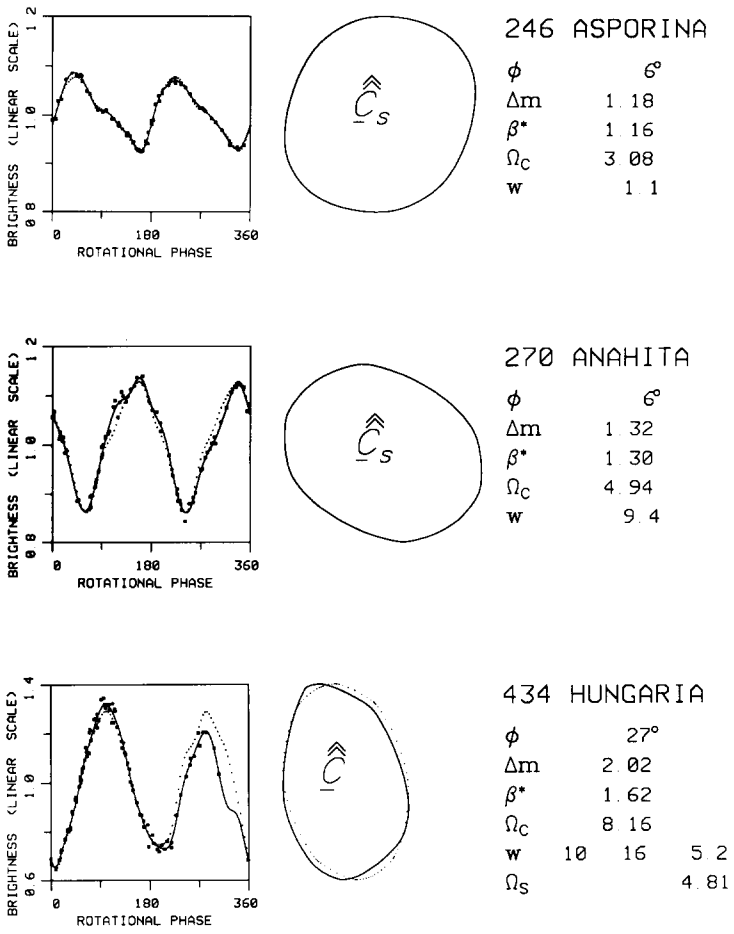

FIG. 15—*Continued.*

which has a weak sixth harmonic. The lightcurve has a significant first harmonic (note the poor fit of $\hat{\mathbf{y}}$ to the lightcurve maxima), which could arise from a nonequatorial view of a nonaxisymmetric shape or, if the shape is axisymmetric and the aspect is equatorial, from a heterogeneous albedo distribution.

1627 Ivar. This lightcurve from Hahn *et al.* (1987) is a composite of data taken during September 1985 at solar phase angles between 18° and 33°; a value of 25° was used in the inversion. Radar data (Ostro *et al.* 1986) and the progression of lightcurve amplitude during the 1985 apparition (A. W. Harris, private communication) suggest that the aspect during September was closer to equatorial than during the closest approach to Earth in July, but that Ivar is actually more elongated than one would infer from any of the lightcurve data or from our estimate of $\underline{C}$.

2156 Kate. Our estimate of this small main-belt asteroid's mean cross section is elongated and highly noncircular. The worst residuals are confined to the minima.

VII. CONCLUSIONS

This paper has been an attempt to formulate and apply a comprehensive framework for using a lightcurve to constrain an asteroid's shape. We have seen that convex-pro-

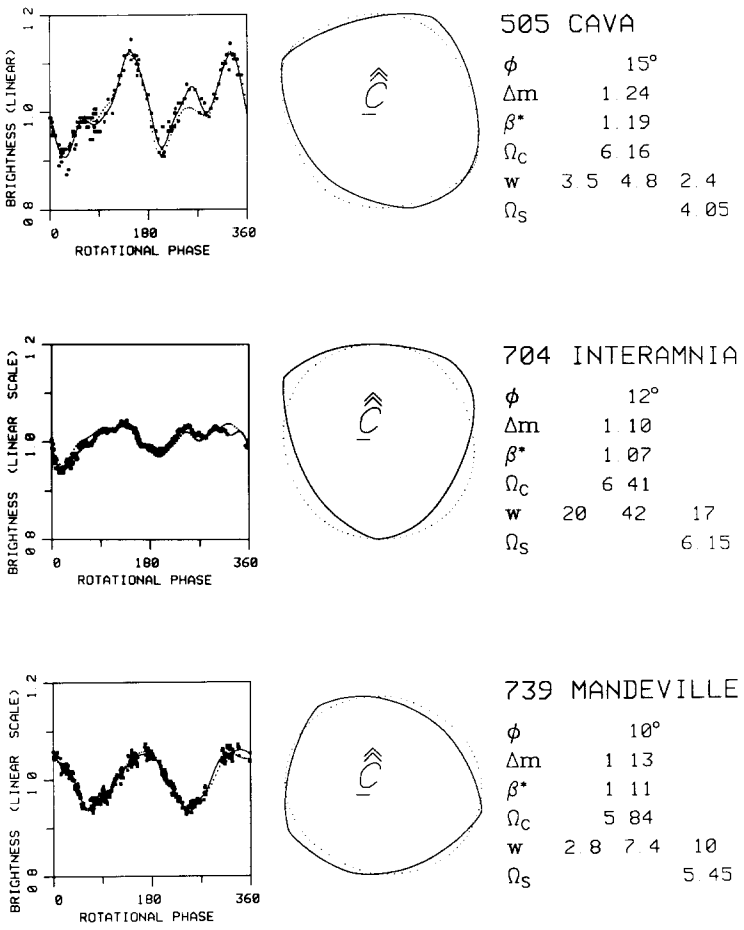

FIG. 15—*Continued.*

file inversion builds on the canonical work of Russell by (i) identifying the mean cross section $\underline{C}$ as the optimal shape constraint available from a lightcurve, (ii) defining the differences between the potential information content of opposition lightcurves and that of nonopposition lightcurves, and (iii) specifying the conditions that determine the accessibility of that information.

The methodology for estimating $\underline{C}$ and $\underline{C}_s$ was introduced by Ostro and Connelly (1984), and here we have tried to assess principal sources of systematic and statistical error. Perhaps the most severe obstacle to estimating the mean cross section stems from violation of Condition GEO. However, it is encouraging that our simulations suggest that salient characteristics of $\hat{\underline{C}}$ resemble those of $\underline{C}$ rather closely for equatorial lightcurves obtained at solar phase angles near 20°, at least for the simplistic shapes we examined. When the viewing/illumination geometry is as much as a few tens of degrees from equatorial, the validity of estimates of $\underline{C}$ or $\underline{C}_s$ should be considered suspect, and simulations like those in Section IV.A can be used to gauge the severity of distortion. (On the other hand, even when $\hat{\underline{C}}$ is apparently biased, it remains a visual representation of the lightcurve in a language befitting the lightcurve's intrinsic information content.)

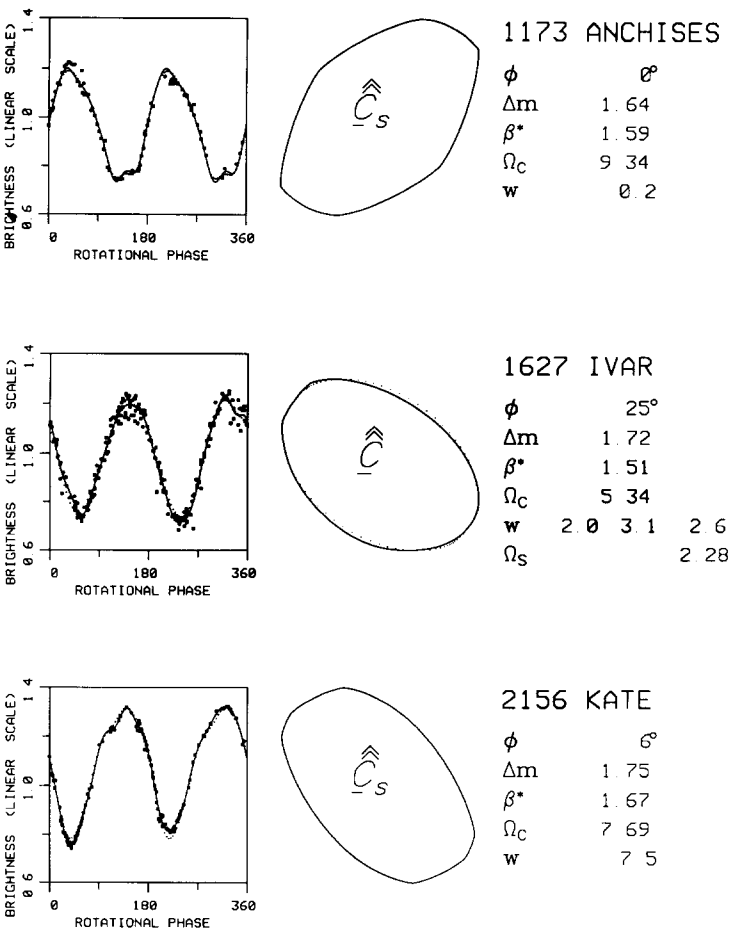

FIG. 15—*Continued.*

We cannot hope to escape the reality that a lightcurve is determined by the viewing/illumination geometry and the surface's light-scattering behavior as well as by the three-dimensional shape. Hopefully, we have demonstrated the value of convex-profile inversion as a tool for assessing the relative roles of each of these factors.

Since shape effects are inextricably involved in the interpretation of *any* disk-integrated observations, including those meant to probe physical properties other than body shape, we conjecture that convex-profile inversion will prove useful in "removing" shape effects in studies designed to constrain those properties. For example, one could apply convex-profile inversion to analysis of an opposition lightcurve to constrain the *average* longitudinal dependence of an asteroid's albedo distribution, as follows. If Condition EVIG is satisfied close to opposition, where Condition GEO is most likely to be satisfied, we can use Russell's Fourier tests to seek evidence for a nonuniform albedo distribution. If the opposition lightcurve has a first harmonic but no higher odd harmonics, we could estimate $\underline{C}_s$ with confidence and attribute residuals between the lightcurve and $\hat{\underline{C}}_s$'s breadth function to albedo variegation. Then one might try to account for those residuals in terms of a nonuniform, two-di-

mensional model asteroid, i.e., by varying the albedos of each side of the polygonal estimate of $\underline{C}_s$ obtained from convex-profile inversion. This exercise would collapse *both* the three-dimensional shape *and* the albedo distribution on the three-dimensional surface into two-dimensional averages, and as such could help to convey the range of possible configurations for the asteroid. Of course, from R3 and R4, we cannot expect lightcurves to reveal *which* of the infinite number of admissible configurations is correct. Unique models of either shape or of the distribution of surface properties simply cannot be obtained from disk-integrated measurements.

If a reliable estimate of an asteroid's mean cross section were available, one could substitute $\hat{\underline{C}}$ for $\hat{\underline{C}}_s$ in the above exercise. It might also be interesting to incorporate Hapke's scattering formalism into this "two-dimensional modeling," as in Section IV.B, to explore the range of possible values for Hapke parameters and perhaps to model effects of surface heterogeneities. At this level of modeling, however, even two-dimensional simplifications cannot be expected to yield unique solutions. Still, these approaches might help to separate shape from compositional variations in analysis of multispectral lightcurves, from regolith thermal characteristics in analysis of thermal–infrared lightcurves, or from surface microstructure in analysis of asteroid "phase functions." The last possibility involves the observation that brightness generally increases as zero phase angle is approached—the opposition effect. In principle, one can use Hapke's scattering theory or any other applicable formalism (e.g., Lumme and Bowell 1981, Goguen 1981) to model phase curves measured for asteroids and then use values of the relevant free parameters to constrain such surface characteristics as porosity. However, any such model necessarily makes *some* assumption about asteroid shape, and convex-profile inversion offers a powerful tool for dealing with shape effects.

In its current incarnation, convex-profile inversion is not readily applicable to data sets consisting of many lightcurves taken under a variety of (nonequatorial) viewing/illumination geometries. To accommodate this most common kind of lightcurve data set, one must parameterize aspects of the asteroid's shape not described by the mean cross section. Satisfactory accomplishment of this task could greatly increase the number of asteroids for which mean cross sections can be accurately estimated and might enhance the value of multi-lightcurve constraints on asteroid pole directions.

ACKNOWLEDGMENTS

We thank B. Hapke and J. Goguen for discussions of the light-scattering properties of particulate surfaces; A. Harris, M. Gaffey, J. Surdej, K. Lumme, and P. Magnusson for critiques of an earlier version of this paper; and L. Belkora, D. Casey, D. Long, and A. Zaruba for technical assistance. Part of this research was conducted at the Jet Propulsion Laboratory, California Institute of Technology, under contract with the National Aeronautics and Space Administration, and part (RC) was supported by NSF Grant MCS77-01740.

REFERENCES

BARUCCI, M. A., AND M. FULCHIGNONI 1982. The dependence of asteroid lightcurves on the orientation parameters and the shapes of asteroids. *Moon Planets* **27,** 47–57.

BARUCCI, M. A., AND M. FULCHIGNONI 1984. On the inversion of asteroidal lightcurve functions. In *Asteroids, Comets, Meteors* (C.-I. Lagerkvist and H. Rickman, Eds.), pp. 101–105. Uppsala University, Uppsala.

BARUCCI, M. A., M. FULCHIGNONI, R. BURCHI, AND V. D'AMBROSIO 1985. Rotational properties of ten main belt asteroids: Analysis of the results obtained by photoelectric photometry. *Icarus* **61,** 152–162.

BINZEL, R. P., AND J. D. MULHOLLAND 1983. A photoelectric lightcurve survey of small main belt asteroids. *Icarus* **56,** 519–533.

BURNS, J. A., AND E. F. TEDESCO 1979. Asteroid lightcurves: Results for rotations and shapes. In *Asteroids* (T. Gehrels, Ed.). Univ. of Arizona Press, Tucson.

CONNELLY, R., AND S. J. OSTRO 1984. Ellipsoids and lightcurves. *Geometriae Dedicata* **17,** 87–98.

DI MARTINO, M., V. ZAPPALÀ, G. DE SANCTIS, AND C. CACCIATORI 1987. Photoelectric photometry of 17 asteroids. *Icarus* **69,** 338–353.

DUNLAP, J. L., AND T. GEHRELS 1969. Minor planets. III. Lightcurves of a Trojan asteroid. *Astron. J.* **74,** 797–803.

DUNLAP, J. L., T. GEHRELS, AND M. L. HOWES 1973.

Minor planets and related objects. IX. Photometry and polarimetry of (1685) Toro. *Astron. J.* **78,** 491–501.

FRENCH, L. M. 1987. Rotation properties of four L5 Trojan asteroids from CCD photometry. *Icarus* **72,** 325–341.

FRENCH, L. M., AND J. VEVERKA 1983. Limb darkening of meteorites and asteroids. *Icarus* **54,** 38–47.

GEHRELS, T. 1956. Photometric studies of asteroids. V. The light-curve and phase function of 20 Massalia. *Astrophys. J.* **123,** 331–338.

GOGUEN, J. 1981. *A Theoretical and Experimental Investigation of the Photometric Functions of Particulate Surfaces.* Ph.D. thesis, Cornell University, Ithaca, NY.

GROENEVELD, I., AND G. P. KUIPER 1954. Photometric studies of asteroids. I. *Astrophys. J.* **120,** 200–220.

HAHN, G., M. DI MARTINO, H. DEBEHOGNE, AND P. MAGNUSSON 1987. Physical studies of Apollo-Amor asteroids: UBVRI photometry of 1036 Ganymed and 1627 Ivar. Manuscript submitted for publication.

HAPKE, B. 1981. Bidirectional reflectance spectroscopy. 1. Theory. *J. Geophys. Res.* **86,** 3039–3054.

HAPKE, B. 1984. Bidirectional reflectance spectroscopy. 3. Correction for macroscopic surface roughness. *Icarus* **59,** 41–59.

HAPKE, B. 1986. Bidirectional reflectance spectroscopy. 4. The extinction coefficient and the opposition effect. *Icarus* **67,** 264–280.

HARRIS, A. W. 1986. Asteroid lightcurve studies. In *Asteroids, Comets, Meteors II* (C.-I. Lagerkvist, B. A. Lindblad, H. Lundstedt, and H. Rickman, Eds.). Uppsala University, Uppsala.

HARRIS, A. W., AND J. W. YOUNG 1980. Asteroid rotation III. 1978 observations. *Icarus* **43,** 20–32.

HARRIS, A. W., AND J. W. YOUNG 1983. Asteroid rotation IV. 1979 observations. *Icarus* **54,** 59–109.

HARRIS, A. W., AND J. W. YOUNG 1985. Photoelectric lightcurve and phase relation of the asteroid 505 Cava. *Icarus* **64,** 528–530.

HARTMANN, W. K., AND D. CRUIKSHANK 1978. The nature of Trojan asteroid 624 Hektor. *Icarus* **36,** 353–366.

HELFENSTEIN, P., AND J. VEVERKA 1987. Photometric properties of lunar terrains derived from Hapke's equation. *Icarus* **72,** 342–257.

LUMME, K., AND E. BOWELL 1981. Radiative transfer in the surfaces of atmosphereless bodies. II. Interpretation of phase curves. *Astrophys. J.* **86,** 1705–1721.

LUSTIG, G., AND G. HAHN 1976. Photoelektrische lichtkurven der planetoiden (2) Pallas und (704) Interamnia. *Acta Phys. Aust.* **44,** 199–205.

MAGNUSSON, P. 1986. Distribution of spin axes and senses of rotation for 20 large asteroids. *Icarus* **68,** 1–39.

OSTRO, S. J., AND R. CONNELLY 1984. Convex profiles from asteroid lightcurves. *Icarus* **57,** 443–463.

OSTRO, S. J., D. B. CAMPBELL, AND I. I. SHAPIRO 1986. Near-Earth asteroids: Radar evidence for extremely irregular, nonconvex shapes. *Eos* **67,** 1078.

PLACKETT, R. L. 1960. *Principles of Regression Analysis.* Oxford Univ. Press (Clarendon), Oxford.

POSPIESZALSKA-SURDEJ, A., AND J. SURDEJ 1985. Determination of the pole orientation of an asteroid. The amplitude–aspect relation revisited. *Astron. Astrophys.* **149,** 186–194.

POUTANEN, M., E. BOWELL, L. J. MARTIN, AND D. T. THOMPSON 1985. Photoelectric photometry of asteroid 69 Hesperia. *Astron. Astrophys. (Suppl.)* **61,** 291–297.

RICHARD, C. W., JR., AND H. HEMAMI 1974. Identification of three-dimensional objects using Fourier descriptors of the boundary curve. *IEEE Trans. Syst. Man Cybernet.* **SMC-4,** 371–378.

RUSSELL, H. N. 1906. On the light-variations of asteroids and satellites. *Astrophys. J.* **24,** 1–18.

SATO, Y., AND I. HONDA 1983. Pseudodistance measures for recognition of curved objects. *IEEE Trans. Pattern Anal. Machine Intelligence* **PAMI-5,** 362–373.

SCALTRITI, F., AND V. ZAPPALÀ 1977. Photoelectric photometry of the minor planets 41 Daphne and 129 Antigone. *Astron. Astrophys.* **56,** 7–11.

SCALTRITI, F., V. ZAPPALÀ, AND R. STANZEL 1978. Lightcurves, phase function and pole of the asteroid 22 Kalliope. *Icarus* **34,** 93–98.

SCHOBER, H. J. 1982. A revised rotation period for the asteroid 164 Eva. *Astron. Astrophys. Suppl.* **48,** 57–62.

STANZEL, R., AND SCHOBER, H. J. 1980. The asteroids 118 Peitho and 952 Caia: Rotation periods and lightcurves from photoelectric observations. *Astron. Astrophys. Suppl.* **39,** 3–5.

VAN HOUTEN-GROENEVELD, I., AND C. J. VAN HOUTEN 1958. Photometric studies of asteroids. VII. *Astrophys. J.* **127,** 253–273.

WEIDENSCHILLING, S. J. 1980. Hektor: Nature and origin of a binary asteroid. *Icarus* **44,** 807–809.

WEIDENSCHILLING, S. J., C. R. CHAPMAN, D. R. DAVIS, R. GREENBERG, D. H. LEVY, AND S. VAIL 1987. Photometric geodesy of main-belt asteroids. I. Observations of 26 large, rapid rotators. *Icarus* **70,** 191–245.

WOOD, H. J., AND G. P. KUIPER 1963. Photometric studies of asteroids. X. *Astrophys. J.* **137,** 1279–1285.

ZAPPALÀ, V., AND Z. KNEŽEVIĆ 1984. Rotation axes of asteroids: Results for 14 objects. *Icarus* **59,** 436–455.

ZAPPALÀ, V., F. SCALTRITI, AND M. DI MARTINO 1983. Photoelectric photometry of 21 asteroids. *Icarus* **56,** 325–344.

ZEIGLER, K. W., AND W. B. FLORENCE 1985. Photoelectric photometry of asteroids 9 Metis, 18 Melpomene, 60 Echo, 116 Sirona, 230 Athamantis, 694 Ekard, and 1984 KD. *Icarus* **62,** 512–517.